co-administration of rAAV-GALR1 and galanin did not affect cell proliferation in either cell line (Fig. 4a).

The ability of GALR signaling to induce apoptosis was assessed by measuring annexin V staining in both cell lines. Co-treatment of cells with rAAV-GALR2 and galanin (1 μM) for 48 h significantly induced apoptosis in 25% of HEp-2 cells, and less markedly induced apoptosis in 16% of KB cells (Fig. 4b).

Furthermore, changes in the cell cycle distribution after activation of either GALR pathway were evaluated by flow cytometry. Co-administration of rAAV-GALR2 vector and galanin (1 μM) for 48 h significantly increased the sub-G0/G1 phase population, to 32% in HEp-2, and to 16.6% in KB cells (Fig. 4c), suggesting that DNA fragmentation was induced by activation of the GALR2 signaling pathway, along with apoptosis. No other effects on cell cycle distribution were observed (Fig. 4c). Additionally, GALR1 activation had no effects on induction of apoptosis or cell cycle distribution (Fig. 4b,c).

**Stimulation of GALR2 signaling downregulates ERK1/2, and upregulates Bim.** As the GALR2-mediated cytotoxic effects were mainly due to apoptosis induction, we examined whether stimulation of the GALR2 signaling pathway affected the phosphorylation states of ERK1/2 and Akt by immunoblotting. Sustained dephosphorylation of ERK1/2 was induced by stimulation of GALR2 signaling in both HNSCC cell lines (Fig. 5a), but no effect on Akt phosphorylation was observed (Fig. 5b).

Moreover, we examined the influence of the pathway on key apoptosis regulators, viz., the Bcl-2 protein and inhibitor of apoptosis protein (IAP) families. The proapoptotic "BH-3–only" Bcl-2 protein Bim was upregulated by activation of GALR2 signaling in HEp-2, but not in KB cells (Fig. 5a,c). No other apoptosis-related proteins investigated were affected by GALR2 activation in either cell line (Fig. 5c). Additionally, activation of GALR1 signaling did not affect the phosphorylation state of ERK or the other apoptotic regulators (Fig. 5c).

**PD98059 inhibits cell proliferation and induces apoptosis via inactivation of the MEK/ERK pathway in HNSCC cells.** To determine whether dephosphorylation of ERK1/2 results in cell growth inhibition and apoptosis induction in HNSCC cells, we examined the reproducibility of GALR2-mediated cytotoxicity using a specific ERK (MEK1) inhibitor, PD98059. As expected, dephosphorylation of ERK1/2 was induced by treatment of both HNSCC cell lines with PD98059 at 20–100 μM for 48 h (Fig. 6a). When cells were cultured in SFM in the presence of PD98059 for 48 h, dose-dependent cell growth suppression (Fig. 6b) and significant apoptosis induction (Fig. 6c) were observed; these effects were more marked in HEp-2 cells. In addition, dose-dependent upregulation of Bim was observed in HEp-2, but not in KB cells, after incubation with PD98059 for 48 h (Fig. 6a). Thus, the GALR2-mediated cytotoxic effects involved at least downregulation of ERK1/2, while Bim may play a role in modulation of GALR2-mediated apoptotic sensitivity. However, despite apoptosis induction in KB cells, Bim activation was not observed, suggesting the existence of multiple signaling pathways for apoptosis induction.

**GALR2-mediated apoptosis is mainly induced via a caspase-independent pathway.** We further investigated the role of the caspase signaling pathway in GALR2-mediated apoptosis by

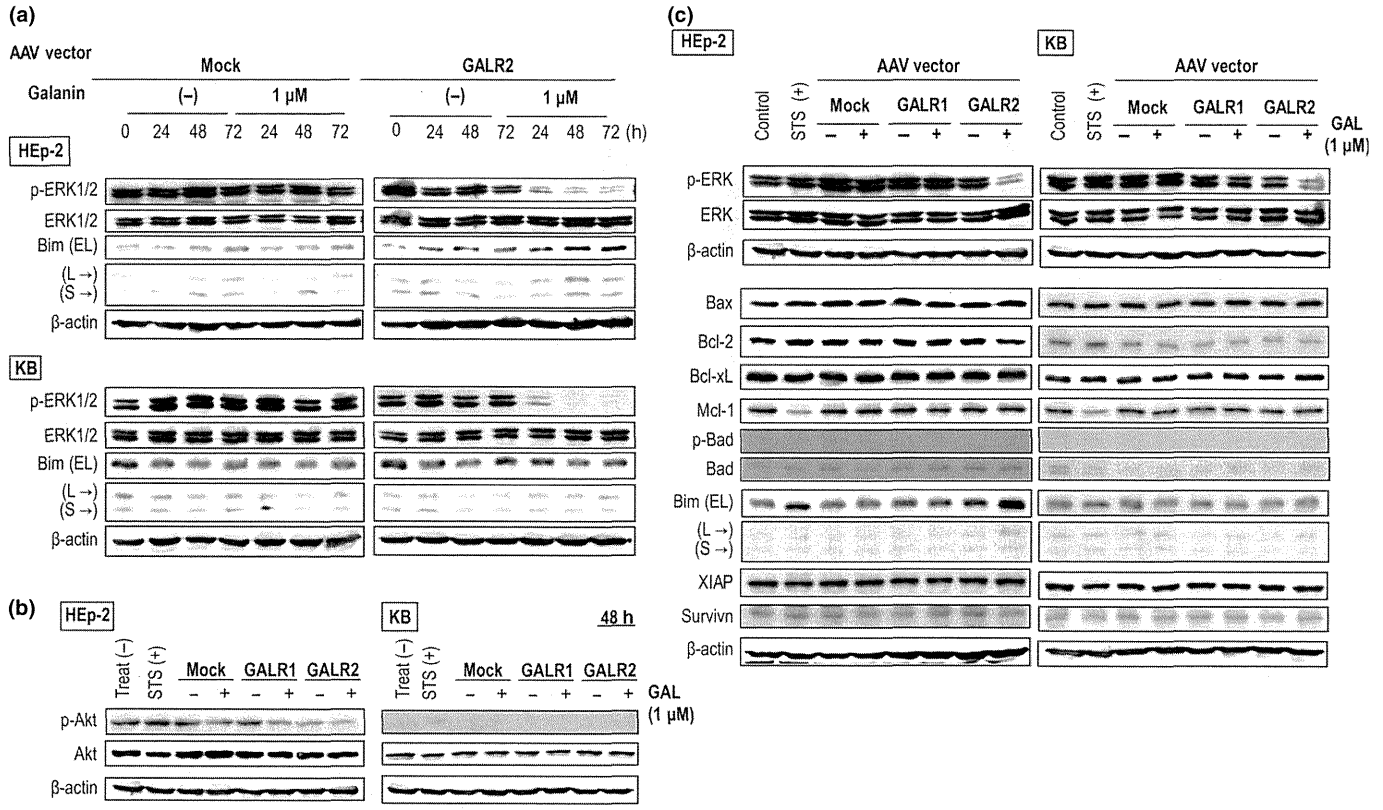


**Fig. 5.** Immunoblotting analysis of the phosphorylation of ERK1/2 and Akt and regulation of key apoptosis regulators by co-administration of recombinant adeno-associated virus (rAAV)-GALR2 vector and galanin. (a) Effect of galanin on ERK1/2 activation and Bim expression in rAAV-GALR2 vector-transduced head and neck squamous cell carcinoma (HNSCC) cells. (b) Effect of galanin on Akt activation in GALR-transduced HNSCC cells. (c) Effects of treatment of cells with galanin and transduction with individual rAAV vectors on the phosphorylation state of ERK1/2 and expression of proteins belonging to the Bcl-2 or IAP families.

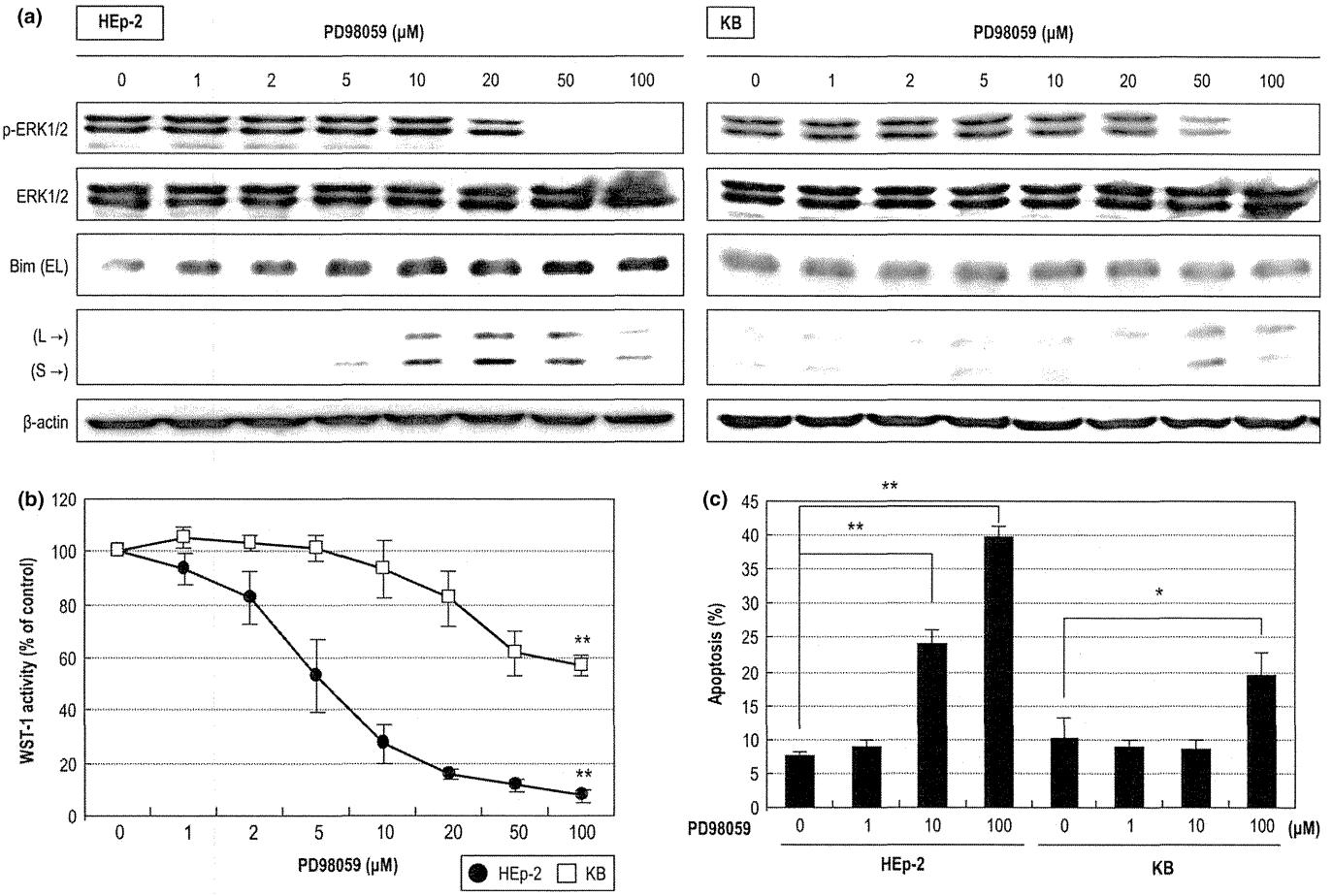


**Fig. 6.** Effect of the MEK inhibitor PD98059 on head and neck squamous cell carcinoma (HNSCC) cells. (a) Phosphorylation states of ERK1/2 after treatment with PD98059. (b) Effect of PD98059 on proliferation of HNSCC cells. (c) Apoptosis analysis by an Annexin V in HNSCC cells. $*P < 0.05$, $**P < 0.01$.

measuring the cleavage of caspase-3 by immunoblotting. Compared to cells treated with 1 μM staurosporine (STS), minimal cleavage of caspase-3 was observed after stimulation of GALR2 signaling pathway in either HNSCC line (Fig. 7a). Additionally, GALR2-mediated inhibition of cell growth was not abrogated by pretreatment with the pan-caspase inhibitor z-VAD-FMK (50 μM) in HEp-2 cells (Fig. 7b).

We further examined whether activation of mitochondrial apoptosis-related factors were involved in initiating a caspase-independent pathway. Apoptosis inducers, such as apoptosis inducing factor (AIF), endonuclease G, HtrA2, and Bit1, are known to be released from the mitochondria to the cytosol and the nucleus by caspase-independent apoptotic signals. No translocation of these proteins in response to GALR2 activation (Fig. 8) was seen in mitochondrial and cytosolic fractions from transduced HEp-2 cells cultured with/without galanin (1 μM) for 48 h.

## Discussion

We previously demonstrated the function of the GALR1 and GALR2 signaling pathways. In HNSCC cell lines, we showed that stably re-expressed GALR1 suppressed tumor cell proliferation via ERK1/2-mediated effects on cyclin-dependent kinase inhibitors, whereas, in GALR2-transduced HNSCC cells, galanin suppressed cell proliferation and induced apoptosis. Thus, we deduced that GALR1 and GALR2 function as tumor suppressors and therefore focused on these proteins as therapeutic targets for HNSCC.

Here, we showed that transduction of GALR2 using rAAV vectors makes HNSCC cells susceptible to galanin-induced growth inhibition and apoptosis; however, we could not show anti-tumor effects of rAAV-mediated GALR1 activation in HNSCC cells. It is unclear why GALR1 and GALR2 have such different effects. We considered that, because of constitutive phosphorylation of ERK1/2 even under serum-free culture conditions in the HNSCC cells used in our experiments, further activation of ERK1/2 by GALR1 activation may not be critical to cell proliferation and survival in these cells.

Although these mechanisms are thought to be partially responsible for tumor cell growth inhibition, the apoptosis induction mechanisms mediated in HNSCC cells by GALR2 activation remain unclear. Our results indicated that downregulation of ERK1/2 is important as a novel apoptotic mechanism triggered by GALR2 activation.

Dephosphorylation of ERK1/2 via stimulation of other GPCRs has previously been reported. Yamada *et al.* reported that angiotensin I type 2 receptor (AT2R) mediated apoptosis followed by dephosphorylation of MAPK in growth factor-supported PC12 cells.[32] Others have reported that inhibition of MAPKs via AT2R was mediated by stimulation of serine/threonine phosphatase 2A (PP2A).[33] It has been reported that phosphotyrosine phosphatase DEP-1/PTPη-dependent dephosphorylation of ERK1/2 is required for inhibition of basic

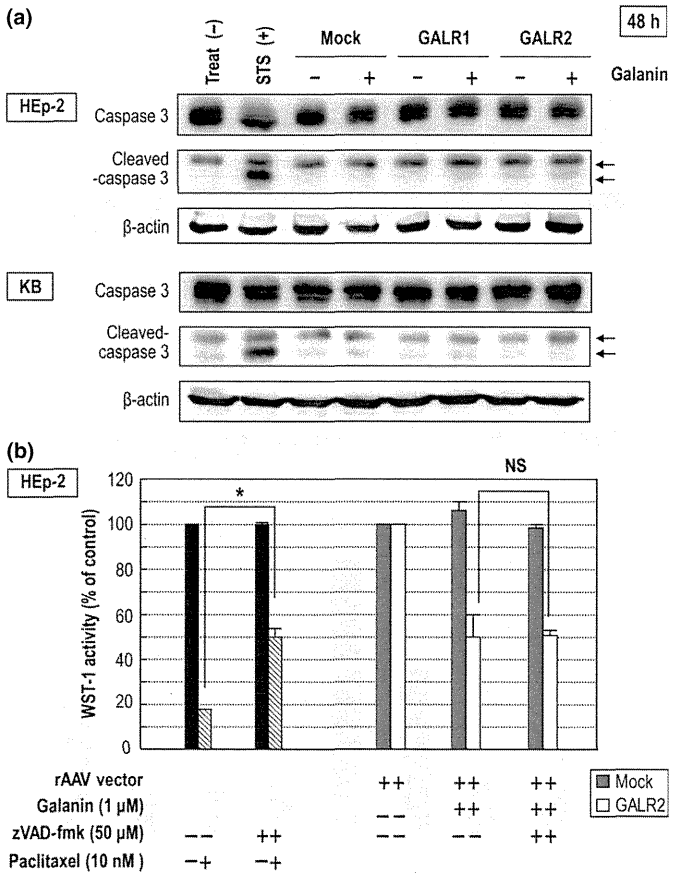


**Fig. 7.** Effect of galanin on the caspase signaling pathway in recombinant adeno-associated virus (rAAV)-GALR2 vector-transduced head and neck squamous cell carcinoma (HNSCC) cells. (a) Assessment of caspase-3 activation by immunoblotting. Staurosporine (STS; 1 μM) for 3 h was used as a positive control for caspase activation. (b) Effect of a pan-caspase inhibitor (z-VAD-fmk) on GALR2-mediated cytotoxic effects in HEp-2 cells. As positive control, to indicate the inhibitory effect of z-VAD-fmk, we used cells exposed to paclitaxel (10 nM) for 48 h.

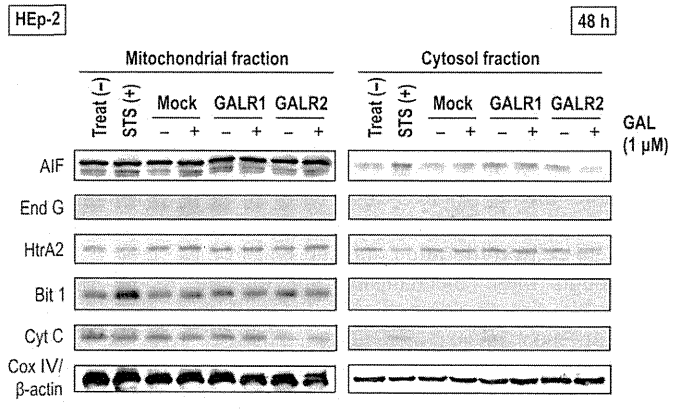


**Fig. 8.** Effects of mitochondrial apoptosis-associated proteins in HEp-2 cell co-administered with each of the recombinant adeno-associated virus (rAAV)-GALR vectors and galanin. Cox IV and β-actin were used as protein-loading controls for the mitochondrial and cytosolic fractions, respectively.

growth factor-dependent cell proliferation mediated by the stimulating somatostatin receptors in glioma cells.[34,35] Therefore, we anticipated that some protein phosphatase related to the dephosphorylation of MAPK cascades may be involved. As an alternative to protein phosphatase activation, Fushimi *et al.* reported that prostaglandin E2 downregulated TNF-α-induced production of matrix metalloproteinase-1 by inhibiting the Raf-1/MEK/ERK cascade through activation of the EP4 prostanoid receptor.[36] Tumor necrosis factor-α–mediated Raf activation, involving phosphorylation at Ser338, was suppressed by stimulation of the EP4 receptor; in contrast, phosphorylation of the inhibitory site on Raf, at Ser259, was stimulated via the EP4 receptor. EP4-mediated Raf inactivation was followed by dephosphorylation of MEK1/2 and ERK1/2. Hence, we examined whether GALR2 activation affects the phosphorylation state of MEK1/2, immediately upstream of ERK1/2. We confirmed that at least dephosphorylation of MEK1/2 was induced by GALR2 activation in HEp-2 cells (data not shown). A comprehensive analysis of the influence of the Ras/Raf/MEK/ERK cascades following activation of the GALR2 signaling pathway requires further study. In addition to the apoptotic mechanisms mediated by MAPK inhibition via specific inhibitors, Eisenmann *et al.* reported the importance of the MAPK pathway-downstream effector protein, RSK, and the BH-3-only proapoptotic protein Bad in melanoma cell survival.[37] Moreover, other groups reported that induction of apoptosis in melanoma cells following inhibition of MEK is mediated by the Bcl-2 family members PUMA, Bim, and Mcl-1, as well as through caspase-independent and AIF-dependent mechanism.[38,39] Therefore, we examined whether these regulators, including those belonging to the Bcl-2 and the IAP family of proteins, and caspase-dependent as well as caspase-independent apoptosis-related proteins, may be associated with the apoptotic mechanisms triggered by GALR2 activation. We found that upregulation of Bim is induced by GALR2 activation. Future studies involving downregulation of Bim expression, for instance by using siRNA, would verify this relationship further.

Although dephosphorylation of ERK1/2 by GALR2 activation was observed in both HNSCC cell lines, significant upregulation of Bim via GALR2 signaling was only induced in HEp-2, but not in KB cells. These results imply that there are both Bim-dependent and Bim-independent unknown pathways that induce apoptosis, and suggest that the type of pathways followed downstream of GALR2 depends on the cell line.

We hypothesize that the reason why the therapeutic effect of AAV-GALR2 in KB cells was less marked than in HEp-2 cells may be that KB cells do not possess the Bim-dependent pathway, whereas HEp-2 cells possess both pathways. Wittau *et al.*[40] demonstrated that there are multiple signaling pathways downstream of GALR2 in small cell lung cancer cells, resulting from coupling of GALR2 to various G-proteins. Their results supported our hypothesis that GALR2 has multiple signaling pathways by which apoptosis is induced, and that ERK inactivation, followed by upregulation of Bim, is associated with the intensity of apoptosis induction following activation of GALR2 signaling.

These findings about differences between in HEp-2 and in KB cells indicate that the pathways involved in GALR2-induced apoptosis diverge, and the details of these signaling pathways remain unclear. For further investigation, we divided GALR2-induced apoptosis pathways into caspase-dependent and -independent pathways in order to investigate this phenomenon further. When investigating the caspase-dependent pathway, we found that GALR2-inhibition of cell growth was not abrogated by the pan-caspase inhibitor z-VAD-FMK. Moreover, none of the apoptosis inducers of the caspase-independent pathway that we examined were translocated to the cytosol from the mitochondria, and activation of members of the IAP and the

Bcl-2 protein families, except for Bim, were unchanged by GALR2 signaling. These results suggested that the apoptotic pathway induced by GALR2 signaling encompasses other unknown pathways. Because carcinogenesis of HNSCC is mainly triggered by extrinsic factors, such as smoking or alcohol, which induce various genetic defects, this distinctive feature makes GALR2 advantageous as a therapeutic gene.

In conclusion, we have shown that GALR2 expression in the presence of galanin induced apoptosis via diverse pathways; thus, gene therapy using the GALR2 gene holds promise as a novel suicide-gene therapy against HNSCC.

## Acknowledgments

We thank Miyoko Mitsu, Satomi Fujiwara and Mikiko Maruta for their technical assistance. This work was supported by a Grant-in-Aid for Scientific Research (Nos. 22591916, 23592539) from the Ministry of Education, Culture, Sports, Science, and Technology of Japan.

## Disclosure Statement

The authors have no conflict of interest.

## References

1 Kamangar F, Dores GM, Anderson WF. Patterns of cancer incidence, mortality, and prevalence across five continents: defining priorities to reduce cancer disparities in different geographic regions of the world. *J Clin Oncol* 2006; **24**: 2137–50.
2 Shibuya K, Mathers CD, Boschi-Pinto C, Lopez AD, Murray CJ. Global and regional estimates of cancer mortality and incidence by site: II. Results for the global burden of disease 2000. *BMC Cancer* 2002; **2**: 37.
3 Choong N, Vokes E. Expanding role of the medical oncologist in the management of head and neck cancer. *CA Cancer J Clin* 2008; **58**: 32–53.
4 Gold KA, Lee HY, Kim ES. Targeted therapies in squamous cell carcinoma of the head and neck. *Cancer* 2009; **115**: 922–35.
5 Tejani MA, Cohen RB, Mehra R. The contribution of cetuximab in the treatment of recurrent and/or metastatic head and neck cancer. *Biologics* 2010; **4**: 173–85.
6 Goerner M, Seiwert TY, Sudhoff H. Molecular targeted therapies in head and neck cancer–an update of recent developments. *Head Neck Oncol* 2010; **2**: 8.
7 Wang F, Arun P, Friedman J, Chen Z, Van Waes C. Current and potential inflammation targeted therapies in head and neck cancer. *Curr Opin Pharmacol* 2009; **9**: 389–95.
8 Kanazawa T, Nishino H, Hasegawa M *et al.* Interleukin-6 directly influences proliferation and invasion potential of head and neck cancer cells. *Eur Arch Otorhinolaryngol* 2007; **264**: 815–21.
9 Hill SJ. G-protein-coupled receptors: past, present and future. *Br J Pharmacol* 2006; **147**(Suppl. 1): S27–37.
10 Kanazawa T, Iwashita T, Kommareddi P *et al.* Galanin and galanin receptor type 1 suppress proliferation in squamous carcinoma cells: activation of the extracellular signal regulated kinase pathway and induction of cyclin-dependent kinase inhibitors. *Oncogene* 2007; **26**: 5762–71.
11 Kanazawa T, Kommareddi PK, Iwashita T *et al.* Galanin receptor subtype 2 suppresses cell proliferation and induces apoptosis in p53 mutant head and neck cancer cells. *Clin Cancer Res* 2009; **15**: 2222–30.
12 Lang R, Gundlach AL, Kofler B. The galanin peptide family: receptor pharmacology, pleiotropic biological actions, and implications in health and disease. *Pharmacol Ther* 2007; **115**: 177–207.
13 Mitsukawa K, Lu X, Bartfai T. Galanin, galanin receptors and drug targets. *Cell Mol Life Sci* 2008; **65**: 1796–805.
14 Berger A, Santic R, Hauser-Kronberger C *et al.* Galanin and galanin receptors in human cancers. *Neuropeptides* 2005; **39**: 353–9.
15 Iishi H, Tatsuta M, Baba M *et al.* Inhibition by galanin of experimental carcinogenesis induced by azaserine in rat pancreas. *Int J Cancer* 1998; **75**: 396–9.
16 El-Salhy M, Starefeldt A. Direct effects of octreotide, galanin and serotonin on human colon cancer cells. *Oncol Rep* 2003; **10**: 1723–8.
17 Tjomsland V, El-Salhy M. Effects of single, double or triple combinations of octreotide, galanin and serotonin on a human pancreatic cancer cell line. *Histol Histopathol* 2005; **20**: 537–41.
18 Kanazawa T, Misawa K, Carey TE. Galanin receptor subtypes 1 and 2 as therapeutic targets in head and neck squamous cell carcinoma. *Expert Opin Ther Targets* 2010; **14**: 289–302.
19 Henson BS, Neubig RR, Jang I *et al.* Galanin receptor 1 has anti-proliferative effects in oral squamous cell carcinoma. *J Biol Chem* 2005; **280**(22): 564–71.
20 Berger A, Lang R, Moritz K *et al.* Galanin receptor subtype GalR2 mediates apoptosis in SH-SY5Y neuroblastoma cells. *Endocrinology* 2004; **145**: 500–7.
21 Tofighi R, Joseph B, Xia S *et al.* Galanin decreases proliferation of PC12 cells and induces apoptosis via its subtype 2 receptor (GalR2). *Proc Natl Acad Sci USA* 2008; **105**: 2717–22.
22 Ozawa K. Gene therapy using AAV. *Uirusu* 2007; **57**: 47–55.
23 Mizukami H, Ozawa K. Utility of AAV vectors derived from novel serotypes. *Yakugaku Zasshi* 2006; **126**: 1021–8.
24 Mingozzi F, High KA. Therapeutic in vivo gene transfer for genetic disease using AAV: progress and challenges. *Nat Rev Genet* 2011; **12**: 341–55.
25 Muramatsu S, Fujimoto K, Kato S *et al.* A phase I study of aromatic L-amino acid decarboxylase gene therapy for Parkinson's disease. *Mol Ther* 2010; **18**: 1731–5.
26 Manno CS, Pierce GF, Arruda VR *et al.* Successful transduction of liver in hemophilia by AAV-Factor IX and limitations imposed by the host immune response. *Nat Med* 2006; **12**: 342–7.
27 Maguire AM, High KA, Auricchio A *et al.* Age-dependent effects of RPE65 gene therapy for Leber's congenital amaurosis: a phase 1 dose-escalation trial. *Lancet* 2009; **374**: 1597–605.
28 Kanazawa T, Mizukami H, Okada T *et al.* Suicide gene therapy using AAV-HSVtk/ganciclovir in combination with irradiation results in regression of human head and neck cancer xenografts in nude mice. *Gene Ther* 2003; **10**: 51–8.
29 Li XP, Li CY, Li X *et al.* Inhibition of human nasopharyngeal carcinoma growth and metastasis in mice by adenovirus-associated virus-mediated expression of human endostatin. *Mol Cancer Ther* 2006; **5**: 1290–8.
30 Jiang M, Liu Z, Xiang Y *et al.* Synergistic antitumor effect of AAV-mediated TRAIL expression combined with cisplatin on head and neck squamous cell carcinoma. *BMC Cancer* 2011; **11**: 54.
31 Kanter-Schlifke I, Toft Sorensen A, Ledri M, Kuteeva E, Hokfelt T, Kokaia M. Galanin gene transfer curtails generalized seizures in kindled rats without altering hippocampal synaptic plasticity. *Neuroscience* 2007; **150**: 984–92.
32 Yamada T, Horiuchi M, Dzau VJ. Angiotensin II type 2 receptor mediates programmed cell death. *Proc Natl Acad Sci USA* 1996; **93**: 156–60.
33 Huang XC, Richards EM, Sumners C. Mitogen-activated protein kinases in rat brain neuronal cultures are activated by angiotensin II type 1 receptors and inhibited by angiotensin II type 2 receptors. *J Biol Chem* 1996; **271**(15): 635–41.
34 Massa A, Barbieri F, Aiello C *et al.* The expression of the phosphotyrosine phosphatase DEP-1/PTPeta dictates the responsivity of glioma cells to somatostatin inhibition of cell proliferation. *J Biol Chem* 2004; **279**(29): 004–12.
35 Barbieri F, Pattarozzi A, Gatti M *et al.* Somatostatin receptors 1, 2, and 5 cooperate in the somatostatin inhibition of C6 glioma cell proliferation in vitro via a phosphotyrosine phosphatase-eta-dependent inhibition of extracellularly regulated kinase-1/2. *Endocrinology* 2008; **149**: 4736–46.
36 Fushimi K, Nakashima S, You F, Takigawa M, Shimizu K. Prostaglandin E2 downregulates TNF-alpha-induced production of matrix metalloproteinase-1 in HCS-2/8 chondrocytes by inhibiting Raf-1/MEK/ERK cascade through EP4 prostanoid receptor activation. *J Cell Biochem* 2007; **100**: 783–93.
37 Eisenmann KM, VanBrocklin MW, Staffend NA, Kitchen SM, Koo HM. Mitogen-activated protein kinase pathway-dependent tumor-specific survival signaling in melanoma cells through inactivation of the proapoptotic protein bad. *Cancer Res* 2003; **63**: 8330–7.
38 Panka DJ, Wang W, Atkins MB, Mier JW. The Raf inhibitor BAY 43-9006 (Sorafenib) induces caspase-independent apoptosis in melanoma cells. *Cancer Res* 2006; **66**: 1611–9.
39 Wang YF, Jiang CC, Kiejda KA, Gillespie S, Zhang XD, Hersey P. Apoptosis induction in human melanoma cells by inhibition of MEK is caspase-independent and mediated by the Bcl-2 family members PUMA, Bim, and Mcl-1. *Clin Cancer Res* 2007; **13**: 4934–42.
40 Wittau N, Grosse R, Kalkbrenner F, Gohla A, Schultz G, Gudermann T. The galanin receptor type 2 initiates multiple signaling pathways in small cell lung cancer cells by coupling to G(q), G(i) and G(12) proteins. *Oncogene* 2000; **19**: 4199–209.

OPEN

Leukemia (2014), 1–11

www.nature.com/leu

ORIGINAL ARTICLE

# Proteasome inhibitors exert cytotoxicity and increase chemosensitivity via transcriptional repression of Notch1 in T-cell acute lymphoblastic leukemia

D Koyama[1], J Kikuchi[1], N Hiraoka[1], T Wada[1], H Kurosawa[2], S Chiba[3] and Y Furukawa[1]

The Notch signaling pathway has been recognized as a key factor for the pathogenesis of T-cell acute lymphoblastic leukemia (T-ALL), because of the high incidence of activating mutations of Notch1. Notch inhibition could serve as a new treatment strategy for T-ALL; however, the attempts to perturb Notch signaling pathways have been unsuccessful so far. In this study, we found that proteasome inhibitors exert cytotoxic effects on T-ALL cells with constitutive activation of Notch1 to a similar extent as myeloma cells. The proteasome inhibitor bortezomib repressed the transcription of Notch1 and downstream effectors including Hes1, GATA3, RUNX3 and nuclear factor-κB (NF-κB) (p65 and p50), coincided with downregulation of the major transactivator Sp1 and its dissociation from Notch1 promoter. Overexpression of the Notch1 intracellular domain (NICD) significantly ameliorated bortezomib-induced cytotoxicity against T-ALL cells. Drug combination studies revealed that bortezomib showed synergistic or additive effects with key drugs for the treatment of T-ALL such as dexamethasone (DEX), doxorubicin and cyclophosphamide, which were readily abolished by NICD overexpression. The synergy of bortezomib and DEX was confirmed *in vivo* using a murine xenograft model. Our findings provide a molecular basis and rationale for the inclusion of proteasome inhibitors in treatment strategies for T-ALL.

*Leukemia* advance online publication, 17 January 2014; doi:10.1038/leu.2013.366

**Keywords:** T-cell acute lymphoblastic leukemia; Notch1; proteasome inhibitor; Sp1; chemosensitization

## INTRODUCTION

T-cell acute lymphoblastic leukemia (T-ALL) is an aggressive hematopoietic malignancy of thymocytes. The disease represents approximately 15% of pediatric and 25% of adult ALL cases. Despite the application of intensive multiagent chemotherapy, the treatment outcome of T-ALL is not satisfactory and the prognosis of relapsed patients is still very poor.[1] Given the limitation of current approaches, it is important to develop new treatment strategies based on increased understanding of the pathophysiology of T-ALL.

Notch1 has been recognized as one of the most important genes in T-ALL pathogenesis, because activating mutations of Notch1 are detected in >50% of T-ALL patients[2–4] and Notch1 overexpression transforms normal hematopoietic stem cells and T-cell progenitors to T-ALL in murine models.[5] Recent investigations suggest that Notch1 is also implicated in drug sensitivity of T-ALL cells.[6,7] It has been reported that the pre-treatment response to glucocorticoids is a major independent factor influencing the survival of ALL patients[8] and the sensitivity to glucocorticoids is negatively correlated with the expression levels of Notch1 in T-ALL cells.[9]

Notch1 is one of four single transmembrane Notch receptors composed of extracellular and intracellular domains that are non-covalently linked via the heterodimerization domains.[10,11] In response to the binding of cognate ligands, Notch receptors are subjected to proteolytic cleavage by γ-secretase, resulting in the liberation of the Notch1 intracellular domain (NICD). Subsequently, NICD translocates to the nuclei and activates the transcription of various genes involved in cell cycle progression, cellular differentiation and apoptosis inhibition.[11,12] In T-ALL, the mutations of Notch1 occur in the proline/glutamic acid/serine/threonine-rich and/or heterodimerization domains to cause constitutive activation of Notch1 via stabilization of NICD and/or ligand-independent generation of NICD.[2,11,12]

On the basis of these findings, γ-secretase inhibitors (GSIs) were expected to be effective for T-ALL because of their ability to block the generation of NICD.[13–15] Unfortunately, most T-ALL cells, especially those with heterodimerization domain mutations, are resistant to GSIs.[2,16] Indeed, clinical trials disclosed the limitation of antitumor activity and a number of severe adverse effects of GSIs.[17,18] In addition, blocking antibodies for specific Notch receptors and/or ligands are also found to be of limited value for the treatment of T-ALL associated with aberrant Notch1 activation.[19–21] Therefore, the development of novel agents targeting the Notch-mediated oncogenic pathway is eagerly awaited.

Proteasome inhibition is now considered a unique and effective way to kill cancer cells that can tolerate conventional chemotherapy. Bortezomib is the first proteasome inhibitor approved for clinical application and is now widely used for the treatment of multiple myeloma (MM).[22] Previous studies showed that bortezomib affects several molecules including nuclear factor-κB (NF-κB) and histone deacetylases (HDACs) in MM cells,[23,24] both of which could be therapeutic targets of T-ALL.[25–28] However, relatively little is known about the cytotoxic activity of

[1]Division of Stem Cell Regulation, Center for Molecular Medicine, Jichi Medical University, Tochigi, Japan; [2]Department of Pediatrics, Dokkyo Medical University, School of Medicine, Tochigi, Japan and [3]Department of Hematology and Tsukuba Advanced Research Alliance, University of Tsukuba, Ibaraki, Japan. Correspondence: Professor Y Furukawa, Division of Stem Cell Regulation, Center for Molecular Medicine, Jichi Medical School, 3311-1 Yakushiji, Shimotsuke, Tochigi 329-0498, Japan.
E-mail: furuyu@jichi.ac.jp
Received 2 August 2013; revised 11 November 2013; accepted 29 November 2013; accepted article preview online 4 December 2013

bortezomib against T-ALL and its mechanisms of action, although a preliminary report suggests the possibility.[29] In this study, we demonstrate that proteasome inhibitors, bortezomib and K-7174, exert marked cytotoxicity against T-ALL cells *in vitro* and *in vivo*, and also increase the sensitivity of T-ALL cells to conventional chemotherapeutic agents via transcriptional repression of Notch1 and downstream effectors such as NF-κB and RUNX3. These findings provide a rationale for the inclusion of proteasome inhibitors in treatment strategies for T-ALL.

## MATERIALS AND METHODS

### Cells and cell culture

We used four *bona fide* human T-ALL cell lines, Jurkat, CEM, MOLT4 and KOPT-K1 (provided by Dr Takeshi Inukai, University of Yamanashi, Yamanashi, Japan), in this study.[2] Other cell lines and their origins are KMS12-BM, U266, RPMI8226 (MM), KOPM30 (B-ALL), HBL-2 (mantle cell lymphoma), Namalwa (Burkitt lymphoma), HL-60 and K562 (acute myeloid leukemia), all of which were purchased from the Health Science Research Resources Bank (Osaka, Japan).

### Drugs

The drugs used in this study and their sources are bortezomib, MLN120B (Millennium Pharmaceuticals, Cambridge, MA, USA), K-7174 (Kowa, Tokyo, Japan), vincristine (Shionogi, Osaka, Japan), doxorubicin (ADM) (Meiji, Tokyo, Japan), mithramycin, dexamethasone (DEX) (Sigma-Aldrich, St Louis, MO, USA), cytosine arabinoside and 4-hydroxycyclophospamide (Wako Biochemicals, Osaka, Japan). All drugs were dissolved in dimethyl sulfoxide at appropriate concentrations and used at a final dilution of 1/1000.

### Cell proliferation assays

Cell proliferation was monitored using a Cell Counting Kit (Wako Biochemicals). In brief, cells were seeded in 96-well flat-bottomed microplates at a density of $1 \times 10^5$ per well and incubated with or without drugs at 37 °C. After incubation, the absorbance was measured at a wavelength of 450 nm using a microplate reader, and expressed as a percentage of the value of corresponding untreated cells.[24]

### Assessment of cell death

Cells were washed with phosphate-buffered saline and stained with phycoerythrin-conjugated annexin-V (annexin-V/PE) (Biovision, Mountain View, CA, USA). Cell death/apoptosis was judged by annexin-V reactivity using a BD LSRFortessa flow cytometer (Becton Dickinson, Bedford, MA, USA).[24]

### Drug combination study

We calculated the combination index of bortezomib and other anti-leukemic drugs using the CompuSyn software and generated isobolograms according to the manufacturer's instructions (www.combosyn.com). The overall effects of drug combination were analyzed by the method of Chou and Talalay.[30]

### Real-time quantitative reverse transcriptase-PCR

Total cellular RNA was isolated from $1 \times 10^5$ cells using an RNeasy Kit (Qiagen, Valencia, CA, USA) and reverse-transcribed into complementary DNA using ReverTra Ace and oligo (dT) primers (Toyobo, Tokyo, Japan). We performed real-time quantitative reverse transcriptase-PCR using the Expression Assays (Hs01062014 for Notch1, Hs00172878 for HES1, Hs00211000 for CYLD, Hs00231122 for GATA3, Hs00231709 for RUNX3, Hs00153294 for RELA, Hs00765730 for NFKB1 and Hs01922876 for glyceraldehyde 3-phosphate dehydrogenase (GAPDH)) and TaqMan Fast Universal PCR Master Mix as described previously.[31]

### Immunoblotting

Immunoblotting was carried out according to the standard method using the following antibodies: anti-Notch1, anti-cleaved Notch1, anti-KLF4, anti-p105/p50, anti-p100/p52, anti-p65, anti-c-Rel, anti-IKKβ, anti-phosphorylated IKKα/β, anti-IκBα (Cell Signaling Technology, Beverly, MA, USA), anti-HDAC1 (Sigma-Aldrich), anti-Sp1, anti-histone H1, anti-MZF-1 and anti-GAPDH (Santa Cruz Biotechnology, Santa Cruz, CA, USA). We used a nuclear extraction kit (Cayman Chemical, Ann Arbor, MI, USA) to separate cytoplasm and nuclear fractions.

### NF-κB assay

NF-κB activity was quantitatively measured as p65 and p50 bound to κB consensus oligonucleotides (5′-AGTTGAGGGGACTTTCCCAGGC-3′) in enzyme-linked immunosorbent assay using the NF-κB Transcription Factor Assay kit (Cayman Chemical).[32]

### Chromatin immunoprecipitation assays

We used the ChIP-IT Express Enzymatic (Active Motif, Carlsbad, CA, USA) to perform chromatin immunoprecipitation assays. In brief, we fixed cells in 1% formaldehyde at room temperature for 10 min and isolated chromatin fractions using enzymatic shearing. After centrifugation, supernatants were incubated with antibodies of interest and protein G magnetic beads at 4 °C overnight. We purified DNA fragments from the mixture according to the manufacturer's instructions and carried out PCR using Mighty Amp (Takara, Shiga, Japan) and the primers depicted in Supplementary Table 1.

### Reporter assays

We amplified the promoter regions of the Notch1 gene (−392 to −1, −342 to −1, −315 to −1 and −300 to −1) using PCR (for primers, see Supplementary Table 1) and inserted them into the pGL4.17 firefly luciferase vector (Promega, Madison, WI, USA) to generate reporter plasmids. We introduced reporter plasmids into CEM cells along with the pGL4.73 *Renilla* luciferase vector (Promega), which served as a positive control to determine transfection efficiencies, using electroporation. After 48 h, firefly and *Renilla* luciferase activities were measured discriminately using the Dual-Luciferase Reporter Assay System (Promega). The promoterless pGL4.17-basic vector was used as a negative control. Luciferase activity was normalized with the internal standard and indicated as a relative ratio to negative controls.

### Lentiviral transduction of NICD in T-ALL cells

The NICD fragment of the Notch1 gene was amplified by PCR using specific primers (forward: 5′-TTCTCGAGCACCATGGTGCTGCTGTCCCG CAAGCG-3′, reverse: 5′-AAGGATCCTTACTTGAAGGCCTCCGGAATG-3′) using complementary DNA from normal T-lymphocyte,[16] and inserted into the CSII-CMV-MCS-IRES2-VENUS vector (provided by Dr Hiroyuki Miyoshi, RIKEN BioResorce Center, Ibaraki, Japan). This vector was co-transfected into 293FT cells with packaging plasmids (Invitrogen, Carlsbad, CA, USA) to produce infective lentiviruses in culture supernatants. Lentiviruses were then added to cell suspensions and transduced for 24 h as previously described.[24] We established stable transformants by isolating single-cell clones using limiting dilution (1 cell per well in 96-well culture plates) after long-term culture. NICD overexpression was verified by immunoblotting for each clone.

### Murine xenograft experiments

We established luciferase-expressing MOLT4 sublines by transfecting the CSII-CMV-MCS-IRES2-VENUS vector-carrying firefly luciferase complementary DNA (provided by Dr Takashi Murakami, Takasaki University of Health and Welfare, Gunma, Japan). Cell suspensions ($1 \times 10^7$ cells in $1 \times 10^{-4}$ l of Iscove's modified Dulbecco's medium) were inoculated subcutaneously into the right thigh of nonobese diabetic/severe combined immunodeficiency (NOD/SCID) mice (Charles River Laboratories, Wilmington, MA, USA) together with $1 \times 10^{-4}$ l Matrigel basement membrane matrix (Becton Dickinson).[16,24] When tumors were measurable after 3–5 days, mice were assigned to four treatment groups receiving the vehicle alone (0.9% NaCl, five times a week), bortezomib alone (0.25 mg/kg twice a week), DEX alone (10 mg/kg five times a week) or bortezomib plus DEX intraperitoneally ($n = 3$–4 in each group). Caliper measurements of the longest perpendicular tumor diameters were performed to estimate the tumor volume using the following formula: $4/3\pi \times (\text{width}/2)^2 \times (\text{length}/2)$, which represents the three-dimensional volume of an ellipse.

Tumor progression was also determined by measuring tumor-derived luciferase activity with the noninvasive bioimaging system. Tumor-bearing mice were injected with the luciferase substrate D-luciferin (1.5 mg/body) intraperitoneally after being anesthetized with isoflurane. Photons transmitted through the body were collected for a specified length of time and analyzed using the IVIS Imaging System with Living Image software (Xenogen, Alameda, CA, USA). Quantitative data were expressed as photon units (photons/s).

## RESULTS

### Proteasome inhibition causes marked cytotoxicity in T-ALL cells

The efficacy of bortezomib for hematological malignancies other than MM and mantle cell lymphoma remains to be determined; therefore, we screened for the cytotoxic effects of bortezomib against different types of hematological malignancies. As shown in Figure 1a, bortezomib was particularly effective for T-ALL cell lines with $IC_{50}$ values of $13.0 \pm 2.9$, $4.5 \pm 0.24$, $3.5 \pm 0.24$ and $4.7 \pm 0.29$ nM for Jurkat, MOLT4, CEM and KOPT-K1, respectively. The $IC_{50}$ values for bortezomib were lower in T-ALL than MM cell lines except for Jurkat. Flow cytometric analysis revealed that growth inhibition was mainly due to the induction of apoptosis but not cell cycle arrest (data not shown). In addition, we found that K-7174, a homopiperazine derivative with a distinct mode of proteasome inhibition from bortezomib,[33,34] was also very effective for T-ALL cell lines including Jurkat (Figure 1a). We confirmed that bortezomib readily inhibited proteasome β5 activity in T-ALL cells in a dose-dependent manner (Supplementary Figure 1). These results suggest that proteasome inhibition has a therapeutic impact on T-ALL as well as MM.

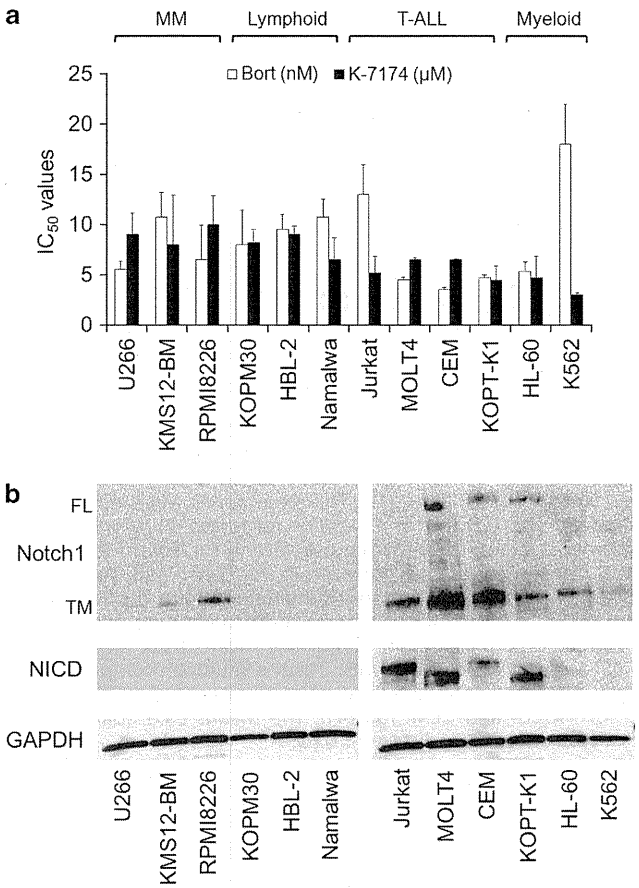


**Figure 1.** Proteasome inhibitors are effective for T-ALL cell lines with constitutive activation of Notch1. (**a**) The $IC_{50}$ values of bortezomib (open column) and K-7174 (filled column) were calculated from dose-response curves of cell lines from various hematological malignancies including MM (U266, KMS12-BM and RPMI 8226), B-lymphoid malignancies (KOPM30, HBL-2 and Namalwa), T-ALL (Jurkat, MOLT4, CEM and KOPT-K1) and myeloid leukemias (HL-60 and K562) obtained at 72 h of culture. (**b**) Whole-cell lysates were prepared from the indicated cell lines and subjected to immunoblotting using specific antibodies that recognize full-length Notch1 (FL), TM and intracellular domain of Notch1 (NICD). The membranes were reprobed with anti-GAPDH antibody to serve as a loading control.

### Bortezomib downregulates the expression of Notch1 in T-ALL cells

Next, we investigated the molecular mechanisms by which proteasome inhibitors affect T-ALL cells using bortezomib, because this drug has already been approved for clinical use in MM and mantle cell lymphoma.[22] The high sensitivity to bortezomib indicates that its targets are critical for T-ALL cell survival, such as Notch1,[2,16] NF-κB[25,26] and HDAC1.[27,28] During the activation of Notch signaling pathways, Notch is proteolytically processed and assembled as heterodimeric proteins composed of an extracellular ligand-binding domain, a single-pass transmembrane domain (TM) and NICD.[10] As NICD in turn translocates to the nucleus and activates the transcription of downstream target genes, the amounts of nuclear NICD reflect the overall activity of Notch signaling pathways. To estimate Notch1 activity, we performed immunoblot analysis for the expression of NICD in various hematopoietic cell lines. As shown in Figure 1b, constitutive activation of Notch1 was exclusively observed in T-ALL cell lines.

We then asked whether bortezomib could target constitutively active Notch1 in T-ALL cells. As shown in Figure 2a, bortezomib markedly inhibited Notch1 activity as evidenced by the disappearance of NICD. The downregulation of NICD was most striking with bortezomib, followed by DEX, among key anti-ALL agents at equitoxic concentrations, suggesting that bortezomib is suitable for therapeutic targeting of Notch1 in T-ALL. Bortezomib readily decreased the expression levels of not only NICD but also full-length Notch1 and TM in a time- and dose-dependent manner (Figures 2b and c). In contrast, bortezomib did not affect the expression of HDAC1, another highly expressed possible therapeutic target of T-ALL (Figure 2c). In addition, bortezomib did not upregulate the expression of CCAAT/enhancer-binding protein homologous protein (data not shown), suggesting that, unlike myeloma cells,[23,34] endoplasmic reticulum stress is not a principal mechanism of bortezomib-mediated cytotoxicity in T-ALL cells.

### Bortezomib suppresses the expression of Notch1 and its targets at transcriptional levels

Next, we determined whether the downregulation of Notch1 expression occurs at transcriptional or post-transcriptional levels in T-ALL cells. We assumed that bortezomib repressed the transcription of the Notch1 gene because of the decrease in the abundance of full-length Notch1 and TM in previous experiments. To validate this assumption, we performed real-time quantitative PCR analysis and confirmed the downregulation of Notch1 mRNA in T-ALL cells during bortezomib treatment (Figure 2d). The extent and kinetics of Notch1 mRNA decrease were well correlated with those at protein levels. We then examined the expression of Notch target genes including HES1,[25,35] GATA3[36] and RUNX3, which was reported to confer drug resistance to T-ALL cells via repression of RUNX1 and PKC-θ.[37] As expected, the expression of Notch direct targets was downregulated by bortezomib coincided with a decrease in Notch1 expression in T-ALL cell lines, except for HES1 in CEM for unknown reasons (Figure 2e). These results imply that bortezomib mainly downregulates Notch1 and its targets at transcriptional levels and thus, would be effective for overcoming drug resistance in T-ALL cells.

### Bortezomib impedes NF-κB activity by affecting the expression of p65 and p50 in T-ALL

It has been reported that NF-κB is activated via NICD/Hes1-mediated repression of the deubiquitinase CYLD and has a crucial role in the survival and drug resistance of T-ALL cells.[25,26] We therefore investigated whether bortezomib impedes NF-κB activity as a consequence of NICD downregulation. Toward this end, we first screened for the expression and localization of the components of NF-κB pathways in T-ALL cell lines. As shown in Figures 3a, p65 and p50 were detected in nuclear fractions and thus, the p65/p50 complex might be constitutively activated in

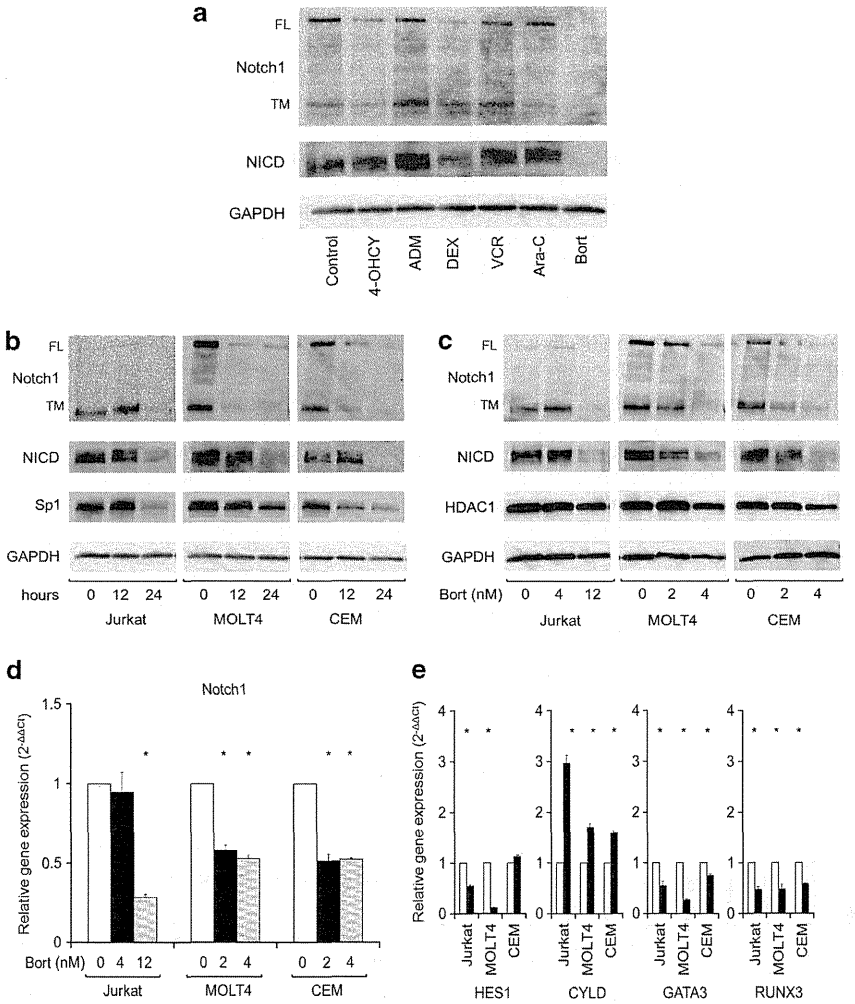


**Figure 2.** Bortezomib downregulates the expression of Notch1 and affects Notch signaling pathways at transcriptional levels in T-ALL cells. (**a**) MOLT4 cells were cultured in the absence (Control) or presence of $IC_{50}$ doses of various anti-leukemia agents (1 μM 4-hydroxycyclophospamide (4-OHCY), 15 nM ADM, 150 nM DEX, 1 nM vincristine (VCR), 5 nM cytosine arabinoside (Ara-C) and 4 nM bortezomib) and subjected to immunoblotting for full-length Notch1 (FL), TM and cleaved Notch1 (NICD) after 24 h. The membranes were reprobed with anti-GAPDH antibody to serve as a loading control. (**b**) T-ALL cells were cultured with bortezomib at $IC_{50}$ (12 nM for Jurkat, 4 nM for MOLT4 and CEM) for up to 24 h. Whole-cell lysates were prepared at the indicated time points and subjected to immunoblotting for Notch1 (FL and TM), NICD, Sp1 and GAPDH. (**c**) T-ALL cells were cultured with the indicated concentrations of bortezomib for 24 h, and subjected to immunoblotting for Notch1 (FL and TM), NICD, HDAC1 and GAPDH. (**d**) Total cellular RNA was isolated simultaneously in the experiments described in (**c**), and subjected to real-time quantitative reverse transcriptase (RT)-PCR. The mRNA expression of Notch1 was normalized to that of GAPDH and quantified by the $2^{-\Delta\Delta Ct}$ method with the values of untreated cells being set at 1.0. The means ± s.d. (bars) of three independent experiments are shown. *P*-values were calculated by one-way analysis of variance with Tukey's multiple comparison test. Asterisks indicate $P<0.05$. (**e**) The mRNA expression of HES1, CYLD, GATA3 and RUNX3 was quantified by real-time quantitative RT-PCR in the indicated cell lines treated with bortezomib at $IC_{50}$ (12 nM for Jurkat, 4 nM for MOLT4 and CEM) for 24 h. The means ± s.d. (bars) of three independent experiments are shown. *P*-values were calculated by Student's *t*-test. Asterisks indicate $P<0.05$.

Jurkat and CEM cells, whereas p65/p65 homodimer seemed to be a dominant complex in MOLT4 cells because of faint expression of p105/p50, which is consistent with previous reports.[29,38] In contrast, these cell lines did not express non-canonical NF-κB components such as c-Rel, p100 and p52.

Having determined NF-κB components expressed in T-ALL cells, we investigated the effects of bortezomib on their abundance and activity. Unexpectedly, bortezomib failed to increase the abundance of IκBα protein (Figures 3b and c), although it restored the expression of CYLD in parallel with HES1 downregulation (Figure 2e). In addition, bortezomib did not only activate IκB kinase β (IKKβ) but decreased its expression levels. In support of this observation, the IKKβ inhibitor MLN120B was rather antagonistic with bortezomib in T-ALL cells, but became synergistic when NICD was overexpressed (Supplementary Figure 2). This could be explained by the negative effect of bortezomib on IKKβ and its restoration by NICD overexpression (data not shown). Instead, bortezomib markedly reduced the amounts of p65 and p50 in a time- and dose-dependent manner (Figures 3b and c). The repression of p50 expression appeared to be mainly transcriptional, because bortezomib decreased the expressions of NFKB1 mRNA and its translational product p105 (Supplementary Figure 3 and Figures 3b and c). In contrast, p65 mRNA expression was unaffected or even increased in MOLT4 cells, implying that bortezomib perturbs the stability of p65 via NICD downregulation as suggested previously.[29,39] As a result of decreased expressions of p65 and p50, canonical NF-κB activity, as detected by the binding of nuclear p65 and p50 to the κB-binding consensus, was considerably reduced in bortezomib-treated T-ALL cells (Figure 3d).

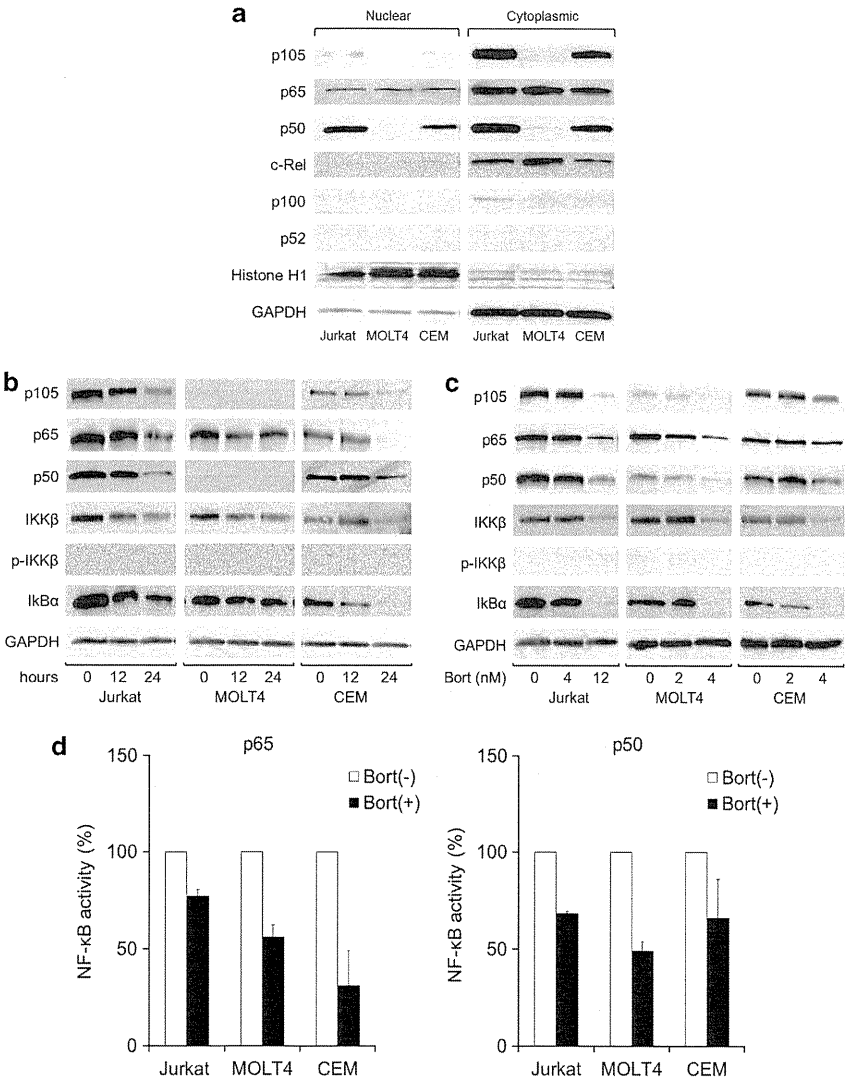


**Figure 3.** Bortezomib inhibits canonical NF-κB activity by downregulating the expression of p65 and p50 in T-ALL cells. (**a**) We extracted nuclear and cytoplasmic fractions from T-ALL cells, and subjected them to immunoblotting for the components of NF-κB pathways. The quality of separation was monitored using histone H1 and GAPDH as nuclear and cytoplasmic markers, respectively. (**b**) We cultured T-ALL cells with bortezomib at $IC_{50}$ (12 nM for Jurkat, 4 nM for MOLT4 and CEM) for the indicated periods and examined the expression of the components of NF-κB pathways using immunoblotting. (**c**) We cultured T-ALL cells with the indicated concentrations of bortezomib for 24 h and examined the expression of the components of NF-κB pathways using immunoblotting. The data shown are representative of multiple independent experiments. (**d**) We cultured T-ALL cells in the absence (open column) or presence (closed column) of bortezomib at $IC_{50}$ (12 nM for Jurkat, 4 nM for MOLT4 and CEM) and prepared nuclear fractions after 24 h. The amounts of p65 and p50 bound to κB consensus sequence (5′-AGTTGAGGGGACTTTCCCAGGC-3′) was quantitatively measured by an enzyme-linked immunosorbent assay using specific antibodies against human p65 and p50.

### Degradation of Sp1 protein underlies transcriptional repression of Notch1 by bortezomib

Next, we investigated the mechanisms of transcriptional repression of the Notch1 gene during bortezomib treatment in T-ALL cells. First, we performed reporter assays to determine bortezomib-responsive regions in the Notch1 promoter. Previously, Lambertini *et al.*[40] reported that the segment between −392 and −1 of the Notch1 gene confers full promoter activity in human keratinocytes. Based on their finding, we constructed four reporter plasmids carrying a full promoter and its deletion fragments (Figure 4a, left panel) and investigated the effects of bortezomib on their activities in T-ALL cells. As shown in Figure 4a, bortezomib significantly reduced the activity of the region −392 to −1 but not others, suggesting that the bortezomib-responsive element is localized in the segment between −392 and −342. This segment is GC-rich (5′-CGGGGAGGCGCAAAGGCGGACGGGGCGTGCGGGAG GAGGTGGCCGCGGAGG-3′) and contains putative binding sites for Sp1, KLF4 and MZF-1 according to database search. Immunoblot analysis revealed that bortezomib markedly downregulated the expression of Sp1, whereas the other two transcription factors were not expressed in T-ALL cells (Figures 2b and 4b). In a previous study, we have shown that Sp1 protein is cleaved and degraded by activated caspase-8 and caspase-3 during bortezomib treatment in MM cells.[24,34] We confirmed the activation of caspase-3 in bortezomib-treated T-ALL cells (data not shown), which might be implicated in Sp1 cleavage and subsequent degradation, and partial restoration of Notch1 downregulation by a specific inhibitor of caspase-3 (Supplementary Figure 4). We further corroborated the importance of Sp1 for Notch1 transcription using mithramycin, which disturbs Sp1 binding to GC

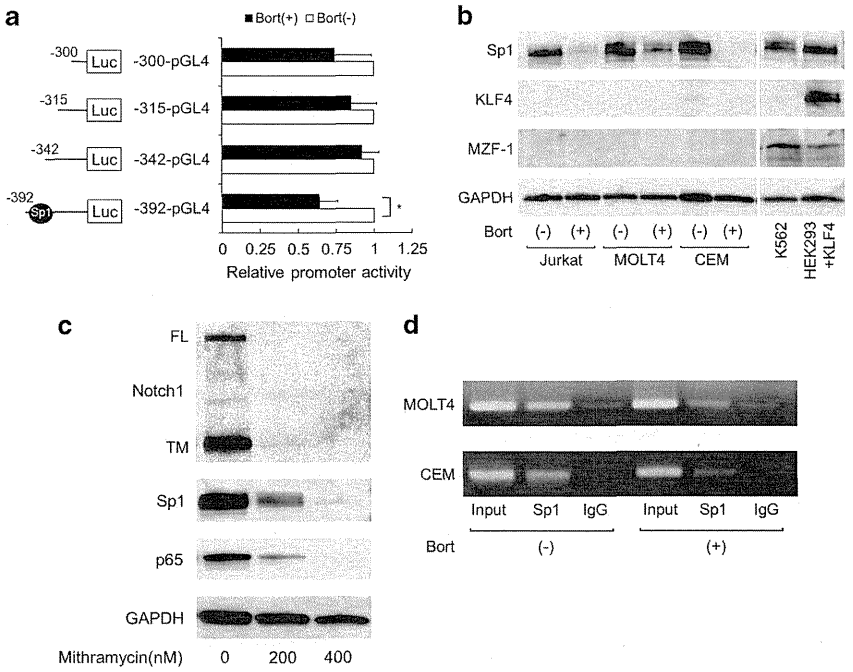


**Figure 4.** Bortezomib decreases Notch1 promoter activity via Sp1 downregulation. (**a**) We transfected 5 μg of pGL4.17 plasmid containing Notch1 promoter sequences between −392 and −1, −342 and −1, −315 and −1, and −300 and −1, respectively, into CEM cells and measured luciferase activities in the absence (open column) or presence (closed column) of 4 nM bortezomib after 48 h. Notch1 promoter activity was calculated as relative firefly luciferase activities against untreated cells after normalization of transfection efficiencies using co-transfected *Renilla* luciferase activities. The means ± s.d. (bars) of three independent experiments are shown. Asterisks indicate $P<0.05$ by Student's *t*-test. (**b**) T-ALL cells were cultured in the absence (−) or presence (+) of bortezomib at $IC_{50}$ (12 nM for Jurkat, 4 nM for MOLT4 and CEM) for 24 h, and subjected to immunoblotting for Sp1, KLF4, MZF-1 and GAPDH (loading control). The antibodies against KLF4 and MZF-1 were validated using HEK293 cells transfected with a KLF4 expression vector and K562 cells as positive controls, respectively. (**c**) Jurkat cells were cultured with mithramycin at the indicated concentrations for 24 h and subjected to immunoblotting using specific antibodies against Notch1 (FL and TM), Sp1, p65 and GAPDH (loading control). (**d**) MOLT4 and CEM cells were cultured in the absence (−) or presence (+) of 4 nM bortezomib, and subjected to chromatin immunoprecipitation assays after 48 h. Chromatin suspensions were immunoprecipitated with anti-Sp1 and corresponding control antibodies (IgG). The precipitants were subjected to PCR to amplify the promoter region (−480 to −342) that includes Sp1-binding sites of the Notch1 gene. The amplified products were visualized by ethidium bromide staining after 2% agarose gel electrophoresis. Representative data of 40 cycles are shown. Input indicates that PCR was performed with genomic DNA.

boxes and induces auto-repression of Sp1 expression.[41,42] Treatment with mithramycin strikingly reduced the abundance of full-length Notch1 and its downstream target p65 in parallel with Sp1 downregulation in T-ALL cells (Figure 4c).

Next, we performed chromatin immunoprecipitation assays to verify the binding of Sp1 to the region between −392 and −342 of Notch1 promoter. Although there are several Sp1 consensus sites in Notch1 promoter, actual binding was detected only in the region between −480 and −342 (Figure 4d and data not shown). Sp1 is dissociated from Notch1 promoter upon bortezomib treatment in MOLT4 and CEM cells, consistent with the findings of reporter assays. Taken together, Sp1 confers the baseline expression of the Notch1 gene and its downregulation by bortezomib leads to transcriptional repression of Notch1 in T-ALL cells.

### Notch1 overexpression rescues T-ALL cells from bortezomib-induced apoptosis

To confirm the dependency of bortezomib action on Notch1 in T-ALL cells, we performed gain-of-function analyses using Jurkat and MOLT4 cells lentivirally transduced with either mock or NICD expression vector (Figure 5a). As shown in Figure 5b, NICD overexpression almost completely abrogated bortezomib-induced apoptosis in both Jurkat and MOLT4 cells. Furthermore, we established NICD-overexpressing stable transformants and confirmed that these cells were resistant to bortezomib in terms of Notch1 downregulation (Figure 5c), NF-kB inactivation (Figures 5c and d) and cytotoxicity (Figure 5e). In addition, NICD overexpression almost completely reversed mithramycin-induced suppression of NF-κB activity (Figure 5d) and apoptosis (Figure 5e), confirming that NICD mostly acts downstream of Sp1. Moreover, NICD overexpression conferred the resistance to not only bortezomib but also other anticancer drugs such as DEX and cytosine arabinoside (Figure 5f). These results indicate that bortezomib induces marked cytotoxicity in T-ALL cells by targeting Notch1-mediated oncogenic pathways involving NF-κB and might modulates the sensitivity to other anticancer agents.

### Combination of bortezomib and other anti-leukemic agents produces synergistic or additive cytotoxicity in T-ALL cells

It has been reported that constitutive activation of Notch signaling pathways underlies the resistance to anticancer drugs and ionizing irradiation in various malignancies.[6,7] We therefore hypothesized that bortezomib-induced suppression of Notch1 enhances the effects of other anti-leukemic agents. To test this hypothesis, we analyzed the combined effects of bortezomib and four key drugs for the treatment of T-ALL using the classical isobologram method.[30] As shown in Figure 6a, the combination index of bortezomib and either DEX or ADM was far below 1.0, indicating a synergistic effect of the combination. The synergistic effect of bortezomib and ADM is fully compatible with the notion that Sp1-mediated p65 overexpression underlies ADM resistance in ALL cells.[43] The combination index of bortezomib and either

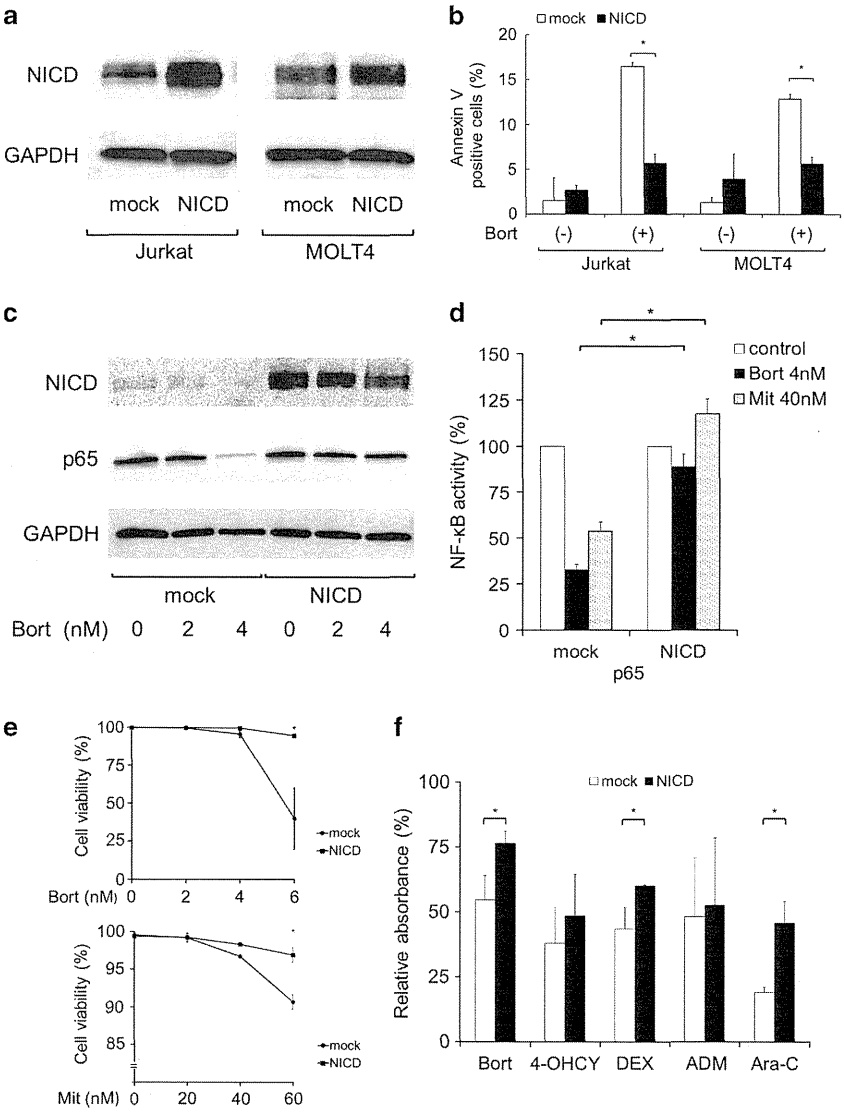


**Figure 5.** Effects of NICD overexpression on bortezomib-induced apoptosis in T-ALL cells. (**a**) Jurkat and MOLT4 cells were lentivirally transduced with either CSII-VENUS (mock) or CSII-VENUS-NICD vector (NICD). Whole-cell lysates were prepared from VENUS-positive cells and subjected to immunoblotting for NICD and GAPDH. (**b**) Mock- and NICD-transduced cells were cultured in the absence (−) or presence (+) of bortezomib at $IC_{50}$ (12 nM for Jurkat and 4 nM for MOLT4) for 48 h and stained with annexin-V/PE in preparation for flow cytometric analysis. The y-axis shows the proportion of annexin-V-positive cells (%) in the VENUS-positive fraction. The means ± s.d. (bars) of three independent experiments are shown. Asterisks indicate $P<0.05$ by Student's *t*-test. (**c**) We established stable transformants from MOLT4 cells lentivirally transduced with either mock or NICD, and examined the expression of NICD, p65 and GAPDH after 24 h of culture with the indicated concentrations of bortezomib. (**d**) NF-κB activity was measured by an enzyme-linked immunsorbent assay for p65 using nuclear extracts from mock- and NICD-transfected MOLT4 cells cultured in the absence (control) or presence of either 4 nM bortezomib (filled column) or 40 nM mithramycin (dotted column) for 24 h. NF-κB activity of untreated controls was set at 100%. The means ± s.d. (bars) of three independent experiments are shown. Asterisks indicate $P<0.05$ by Student's *t*-test. (**e**) We cultured MOLT4 stable transformants (mock and NICD) with the indicated concentrations of either bortezomib (upper panel) or mithramycin (lower panel) for 48 h and stained with annexin-V/PE in preparation for flow cytometry. The y axis shows cell viability calculated by the equation: 100–annexin-V positivity (%). The means ± s.d. (bars) of three independent experiments are shown. Asterisks indicate $P<0.05$ by Student's *t*-test. (**f**) We treated MOLT4 stable transformants (mock and NICD) with the indicated drugs and evaluated cell proliferation using MTT assays after 72 h. The proliferation of untreated cells was set at 100%. The means ± s.d. (bars) of three independent experiments are shown. Asterisks indicate $P<0.05$ by Student's *t*-test.

cytosine arabinoside or 4-hydroxycyclophospamide was around 1.0, suggesting an additive or sub-additive effect of the combination.

Recently, Cialfi *et al.*[9] reported that glucocorticoids induce transcriptional repression of the Notch1 gene through glucocorticoid-responsive elements. As glucocorticoid-responsive elements (–1995, –1075, –978 and –873) are located far upstream of major Sp1-binding sites (–392/–342), it is highly likely that bortezomib and glucocorticoids synergistically repress transcription of Notch1 in T-ALL cells. Immunoblot analysis showed that this was the case: DEX readily potentiated bortezomib-induced suppression of all forms of Notch1 (FL, TM and NICD) in a dose-dependent manner (Figure 6b). Similarly, ADM greatly enhanced bortezomib-induced downregulation of Notch1 especially NICD, although ADM alone did not affect the expression of Notch1 at all. These results suggest that NICD targeting underlies the synergistic effects of bortezomib and these agents. In support of this view, we demonstrated that NICD overexpression abolished the synergistic

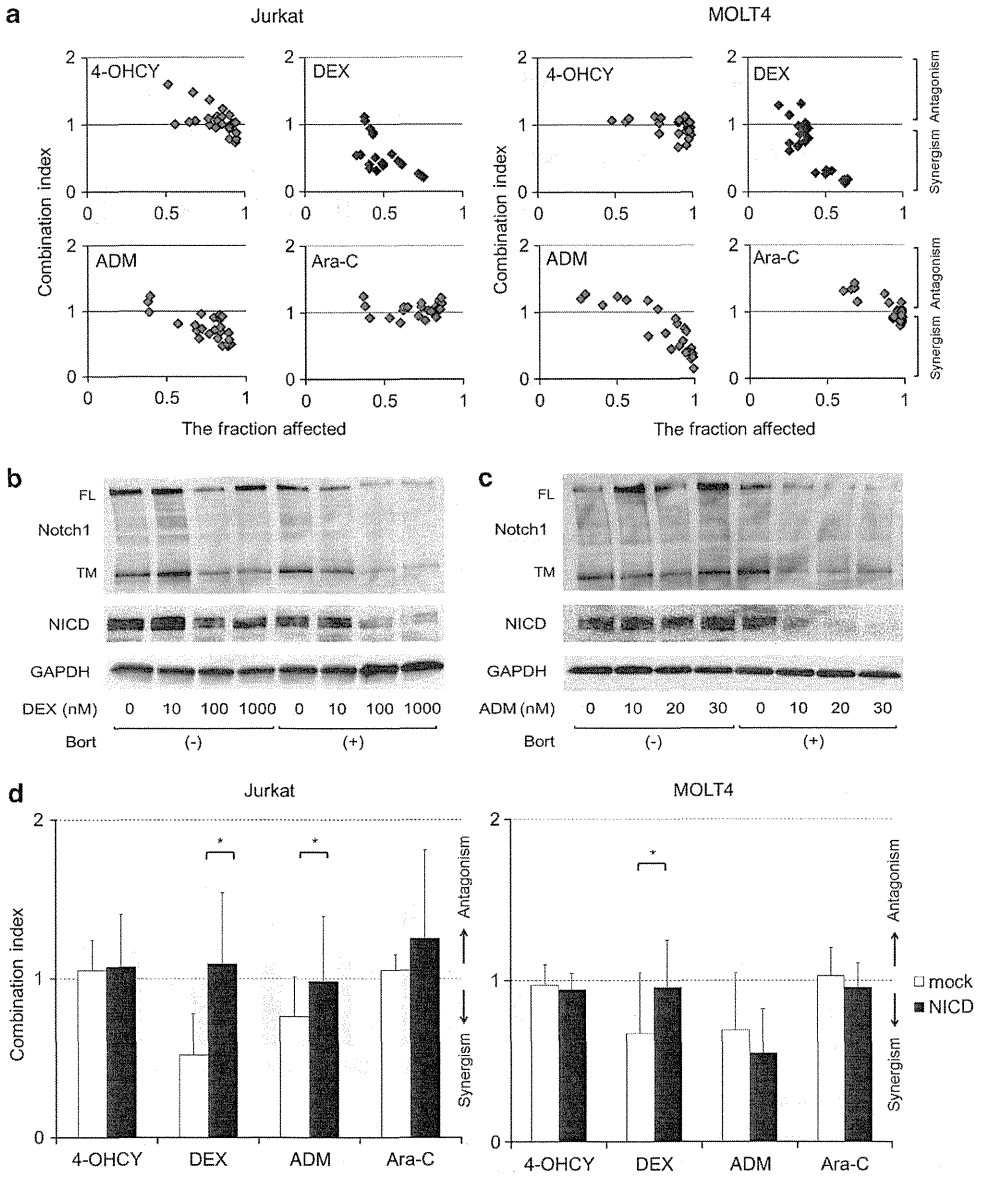


**Figure 6.** Synergistic or additive effects of bortezomib and other anti-leukemia drugs on T-ALL cells *in vitro*. (**a**) Jurkat and MOLT4 cells were treated with various anti-leukemia drugs in the absence or presence of bortezomib for 72 h to obtain dose-response curves of each combination. The combination index plots were generated by the CompuSyn software according to the method of Chou and Talalay. Combination index $<1.0$ means synergism of the two drugs. (**b**) MOLT4 cells were cultured in the absence (−) or presence (+) of 3 nM bortezomib and various doses (0–1000 nM) of DEX for 48 h, and subjected to immunoblotting for full-length Notch1 (FL), Notch1 TM, cleaved Notch1 (NICD) and GAPDH (internal control). (**c**) MOLT4 cells were cultured in the absence (−) or presence (+) of 3 nM bortezomib and various doses (0–30 nM) of doxorubicin (ADM) for 48 h, and subjected to immunoblotting for full-length Notch1 (FL), Notch1 TM, cleaved Notch1 (NICD) and GAPDH (internal control). (**d**) Mock- or NICD-carrying stable transformants of Jurkat and MOLT4 were treated with various anti-leukemia drugs in the absence or presence of bortezomib for 72 h to obtain dose-response curves of each combination. The combination index was calculated by the CompuSyn software according to the method of Chou and Talalay. Combination index $<1.0$ means synergism of the two drugs. The means ± s.d. (bars) of three independent experiments are shown. Asterisks indicate $P<0.05$ by Student's *t*-test.

effects of bortezomib and either DEX or ADM in Jurkat and MOLT4 stable transformants (Figure 6d). Furthermore, the Sp1 inhibitor mithramycin was also synergistic with the same set of agents as bortezomib in T-ALL cells (Supplementary Figure 5). Taken together, bortezomib could elicit an anti-leukemic effect alone or in combination with conventional drugs on T-ALL cells by targeting the Sp1/Notch1 pathway.

### Synergistic anti-leukemia effects of bortezomib and DEX *in vivo*

Finally, we validated therapeutic effects of bortezomib alone and in combination with DEX on T-ALL *in vivo*. For this purpose, we inoculated MOLT4 cells into NOD/SCID mice and treated them in four ways: the vehicle alone, DEX alone, bortezomib alone and the combination of both agents. As shown in Figure 7a, inoculated tumors rapidly grew in vehicle control mice between 7 and 14 days. Monotherapy with either DEX or bortezomib was able to retard tumor growth, but the effect of combination was striking with the almost complete disappearance of inoculated tumors in some recipients (Figures 7b–d). These observations confirm the results of *in vitro* experiments and further suggest that combination therapy including bortezomib is effective for T-ALL in clinical settings.

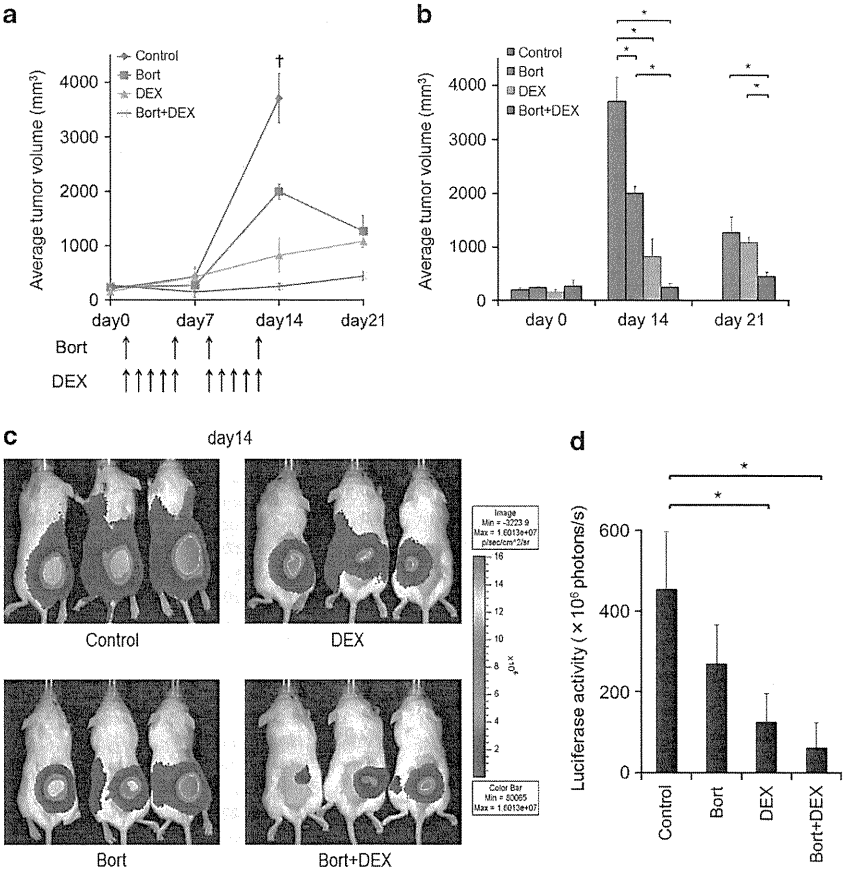


**Figure 7.** Synergistic effects of bortezomib and DEX on T-ALL cells *in vivo*. (**a**) We inoculated $1 \times 10^7$ MOLT4 cells into NOD/SCID mice and treated them in four ways: the vehicle alone (Control), DEX alone (DEX), bortezomib alone (Bor) and the combination of both agents (Bor + DEX). Treatments were started at day 0 when inoculated tumors were measurable. Tumor sizes were measured at the indicated time points to calculate tumor volume. (**b**) The y axis shows the average tumor volume at days 0, 14 and 21. The means ± s.d. (bars) are shown ($n = 3$–4). *P*-values were calculated by one-way analysis of variance (ANOVA) with the Tukey's multiple comparison test (*$P < 0.05$). (**c**) We inoculated $1 \times 10^7$ luciferase-expressing MOLT4 sublines into NOD/SCID mice and treated as described in (**a**). *In vivo* luciferase activity was measured by the IVIS Imaging System at day 14. (**d**) Quantitative data of *in vivo* bioluminescence imaging expressed as photon units (photons/s). The means ± s.d. (bars) are shown ($n = 3$). *P*-values were calculated by one-way ANOVA with the Tukey's multiple comparison test (*$P < 0.05$).

## DISCUSSION

In this study, we demonstrated that proteasome inhibitors effectively target constitutively active Notch1 to elicit cytotoxicity and increase drug sensitivity in T-ALL cells *in vitro* and *in vivo*. In contrast to GSIs, bortezomib is highly effective for T-ALL cells regardless of the presence of mutations at heterodimerization domains, because it downregulates the expression of Notch1 at a transcriptional level via degradation of Sp1, a pivotal transactivator of the Notch1 gene. This point is obviously advantageous over other Notch-targeting agents including GSIs and blocking antibodies against extracellular domains of Notch1. The reduction of NICD is not only cytotoxic to T-ALL cells but also enhances their sensitivity to other anti-leukemia drugs including glucocorticoids and doxorubicin. This is fully consistent with a previous finding that GSI-mediated inhibition of Notch signaling reverses glucocorticoid resistance in T-ALL cells.[6] The safety and effectiveness of bortezomib were already established through long-term clinical experience.[22] Taken together, this study provides a strong rationale for the inclusion of bortezomib in multidrug combination therapy for T-ALL patients to improve the treatment outcome and prognosis.

It is still possible that post-transcriptional mechanisms are also involved in Notch1 downregulation by proteasome inhibitors. It has been reported that Notch1 is cleaved into six fragments mainly by caspase-6 in dying T-lymphocytes.[44] Moreover, Notch1 signaling is reported to be affected by lysosome activity.[45] We therefore examined the effects of the caspase-6 inhibitor Z-VEID-fmk and the lysosome inhibitor chloroquine on Notch1 expression in bortezomib-treated T-ALL cells. We found no evidence of participation of these pathways in bortezomib-induced downregulation of Notch1 (data not shown). From these results, we provisionally concluded that bortezomib-induced decrease in Notch1 expression primarily occurs at a transcriptional level in T-ALL cells.

Downregulation of Sp1 seems to be responsible for transcriptional repression of Notch1 in bortezomib-treated T-ALL cells; however, the presence of additional mechanisms cannot be ruled out. Sp1 is known to undergo post-translational modifications such as phosphorylation, glycosylation, acetylation, sumoylation and ubiquitination.[46] After sumoylation, Sp1 is ubiquitinated by the ubiquitin E3 ligase RNF4 and is degraded via ubiquitin-proteasome cascades. Bortezomib could inhibit this process to accumulate ubiquitinated Sp1, which perturbs the function of residual unmodified Sp1 in T-ALL cells. It is worth investigating that bortezomib inactivates the transcription of Sp1 target genes including Notch1 by perturbing the activator function of Sp1 via post-translational mechanisms.

Accumulating evidence indicates that Notch activates NF-κB pathways via multiple mechanisms. In CD3/CD28-stimulated murine T-lymphocytes, NICD directly binds to c-Rel and p50, and facilitates their nuclear retention by competing with IκBα.[47] Forced expression of NICD reportedly induces nuclear translocation of p65, p50, c-Rel and RelB in hematopoietic progenitor cells.[39] These observations are in line with our finding that NICD downregulation resulted in a decreased expression of p65 and p50 in the nuclei, although the underlying mechanisms are to be elucidated. It was demonstrated that NICD activates the IKK complex via CYLD downregulation[25,26] or direct interaction[39] to trigger proteasome-dependent degradation of IκBα, leading to canonical NF-κB activation. It is possible that bortezomib reverses this process by targeting NICD to increase the abundance of IκBα, but our data did not support this view. Bortezomib was shown to activate IKKβ and decrease the abundance of IκBα, thereby increasing canonical NF-kB activity in myeloma cells;[23] however, this was not reproducible in T-ALL cells. In T-ALL cells, bortezomib-mediated NICD downregulation perturbs IKKβ activity via destabilization of the IKK complex, but fails to increase the abundance of IκBα because of concomitant repression of the IκBα gene, a direct transcriptional target of NICD.[39] In this regard, the synergistic effect of bortezomib and an IKK inhibitor in NICD-overexpressing cells is reasonable and offers the possibility of clinical translation of this combination in bortezomib refractory cases.[48]

The emerging question here is why downregulation of Sp1, which is widely expressed and activates the transcription of numerous genes including housekeepers, results in a selective repression of Notch1 with less effect on the transcription of other genes such as HDAC1 and GAPDH. A recent elegant study by Lovén *et al.*[49] provides a good explanation. In cancer cells, the expression of genes harboring oncogenic mutations is driven by a unique element designated as super-enhancers, where a high level of multiple transcription factors and coactivators accumulate at a relatively wide distance. The super-enhancers are extremely susceptible to subtle changes in activator concentrations because of the high demand of cooperative binding and synergistic activation by their components. In case of T-ALL, the expression of its driver gene Notch1 might be sustained by Sp1 binding to super-enhancer at the region between −480 and −342, and thus, is extremely vulnerable to the loss of Sp1 by proteasome inhibitors. Nonetheless, addiction to Sp1 was demonstrated in cancer cells before the proposal of the concept of super-enhancers.[24,40,50] As pointed out by Lovén *et al.*,[49] super-enhancers are ideal therapeutic targets of various intractable cancers including MM and T-ALL.

## CONFLICT OF INTEREST

YF received research funding and honoraria from Janssen Pharmaceuticals K.K. and Novartis Pharmaceuticals Co. The remaining authors declare no conflict of interest.

## ACKNOWLEDGEMENTS

This work was supported in part by the High-Tech Research Center Project for Private Universities: Matching Fund Subsidy from MEXT, a Grant-in-Aid for Scientific Research from JSPS and research grants from Japan Leukemia Research Fund, Takeda Science Foundation, the Naito Foundation, the Yasuda Medical Foundation, Mitsui Life Social Welfare Foundation and the Uehara Memorial Foundation (to JK and YF).

## REFERENCES

1 Pui CH, Evans WE. Treatment of acute lymphoblastic leukemia. *N Engl J Med* 2006; **354**: 166–178.
2 Weng AP, Ferrando AA, Lee W, Morris JP, Silverman LB, Sanchez-Irizarry C *et al.* Activating mutations of NOTCH1 in human T cell acute lymphoblastic leukemia. *Science* 2004; **306**: 269–271.
3 Callens C, Baleydier F, Lengline E, Abdelali RB, Petit A, Villarese P *et al.* Clinical impact of *NOTCH1* and/or *FBXW7* mutations, *FLASH* deletion, and *TCR* status in pediatric T-cell lymphoblastic lymphoma. *J Clin Oncol* 2012; **30**: 1966–1973.
4 Jenkinson S, Koo K, Mansour MR, Goulden N, Vore A, Mitchell C *et al.* Impact of NOTCH1/FBXW7 mutations on outcome in pediatric T-cell acute lymphoblastic leukemia patients treated on the MRC UKALL 2003 trial. *Leukemia* 2013; **27**: 41–47.
5 Pear WS, Aster JC, Scott ML, Hasserjian RP, Soffer B, Sklar J *et al.* Exclusive development of T cell neoplasms in mice transplanted with bone marrow expressing activated Notch alleles. *J Exp Med* 1996; **183**: 2283–2291.
6 Real PJ, Tosello V, Palomero T, Castillo M, Hernando E, de Stanchina E *et al.* γ-Secretase inhibitors reverse glucocorticoid resistance in T cell acute lymphoblastic leukemia. *Nat Med* 2009; **15**: 50–58.
7 Wang Z, Li Y, Ahmad A, Azmi AS, Banerjee S, Kong D *et al.* Targeting Notch signaling pathway to overcome drug resistance for cancer therapy. *Biochim Biophys Acta* 2010; **1806**: 258–267.
8 Annino L, Vegna ML, Camera A, Specchia G, Visani G, Floritoni G *et al.* Treatment of adult acute lymphoblastic leukemia (ALL): long-term follow-up of the GIMEMA ALL 0288 randomized study. *Blood* 2002; **99**: 863–871.
9 Cialfi S, Palermo R, Manca S, Checquolo S, Bellavia D, Pelullo M *et al.* Glucocorticoid sensitivity of T-cell lymphoblastic leukemia/lymphoma is associated with glucocorticoid receptor-mediated inhibition of Notch1 expression. *Leukemia* 2013; **27**: 485–488.
10 Koch U, Radtke F. Notch in T-ALL: new players in a complex disease. *Trends Immunol* 2011; **32**: 434–442.
11 Lobry C, Oh P, Aifantis I. Oncogenic and tumor suppressor functions of Notch in cancer: it's NOTCH what you think. *J Exp Med* 2011; **208**: 1931–1935.
12 Sanchez-Irizarry C, Carpenter AC, Weng AP, Pear WS, Aster JC, Blacklow SC. Notch subunit heterodimerization and prevention of ligand independent proteolytic activation depend, respectively, on a novel domain and the LNR repeats. *Mol Cell Biol* 2004; **24**: 9265–9273.
13 Osipo C, Patel P, Rizzo P, Clementtz AG, Hao L, Golde TE *et al.* ErbB-2 inhibition activates Notch-1 and sensitizes breast cancer cells to a γ-secretase inhibitor. *Oncogene* 2008; **27**: 5019–5032.
14 Akiyoshi T, Nakamura M, Yanai K, Nagai S, Wada J, Koga K *et al.* γ-Secretase inhibitors enhance taxane-induced mitotic arrest and apoptosis in colon cancer cells. *Gastroenterology* 2008; **134**: 131–144.
15 Meng RD, Shelton CC, Li Y-M, Qin L-X, Notterman D, Paty PB *et al.* γ-Secretase inhibitors abrogate oxaliplatin-induced activation of the Notch-1 signaling pathway in colon cancer cells resulting in enhanced chemosensitivity. *Cancer Res* 2009; **69**: 573–582.
16 Masuda S, Kumano K, Suzuki T, Tomita T, Iwatsubo T, Natsugari H *et al.* Dual antitumor mechanisms of Notch signaling inhibitor in a T-cell acute lymphoblastic leukemia xenograft model. *Cancer Sci* 2009; **100**: 2444–2450.
17 Krop I, Demuth T, Guthrie T, Wen PY, Mason WP, Chinnaiyan P *et al.* Phase I pharmacologic and pharmacodynamic study of the gamma secretase (Notch) inhibitor MK-0752 in adult patients with advanced solid tumors. *J Clin Oncol* 2012; **30**: 2307–2313.
18 Tolcher AW, Messersmith WA, Mikulski SM, Papadopoulos KP, Kwak EL, Gibbon DG *et al.* Phase I study of RO4929097, a gamma secretase inhibitor of Notch signaling, in patients with refractory metastatic or locally advanced solid tumors. *J Clin Oncol* 2012; **30**: 2348–2353.
19 Li K, Li Y, Wu W, Gordon WR, Chang DW, Lu M *et al.* Modulation of Notch signaling by antibodies specific for the extracellular negative regulatory region of NOTCH3. *J Biol Chem* 2008; **283**: 8046–8054.
20 Wu Y, Cain-Hom C, Choy L, Hagenbeek TJ, de Leon GP, Chen Y *et al.* Therapeutic antibody targeting of individual Notch receptors. *Nature* 2010; **464**: 1052–1057.
21 Aste-Amézaga M, Zhang N, Lineberger JE, Arnold BA, Toner TJ, Gu M *et al.* Characterization of Notch1 antibodies that inhibit signaling of both normal and mutated Notch1 receptors. *PLoS One* 2010; **5**: e9094.
22 Moreau P, Richardson PG, Cavo M, Orlowski RZ, San Miguel JF, Palumbo A *et al.* Proteasome inhibitors in multiple myeloma: 10 years later. *Blood* 2012; **120**: 947–959.
23 Hideshima T, Ikeda H, Chauhan D, Okawa Y, Raje N, Podar K *et al.* Bortezomib induces canonical nuclear factor-κB activation in multiple myeloma cells. *Blood* 2009; **114**: 1046–1052.
24 Kikuchi J, Wada T, Shimizu R, Izumi T, Akutsu M, Mitsunaga K *et al.* Histone deacetylases are critical targets of bortezomib-induced cytotoxicity in multiple myeloma. *Blood* 2010; **116**: 406–417.
25 Espinosa L, Cathelin S, D'Altri T, Trimarchi T, Statnikov A, Guiu J *et al.* The Notch/Hes1 pathway sustains NF-κB activation through *CYLD* repression in T cell leukemia. *Cancer Cell* 2010; **18**: 268–281.
26 D'Altri T, Gonzalez J, Aifantis I, Espinosa L, Bigas A. Hes1 expression and CYLD repression are essential events downstream of Notch1 in T-cell leukemia. *Cell Cycle* 2011; **10**: 1031–1036.

27 Moreno DA, Scridel CA, Cortez MAA, de Paula Queiroz R, Valera ET, da Silva Silveira V *et al.* Differential expression of *HDAC3*, *HDAC7* and *HDAC9* is associated with prognosis and survival in childhood acute lymphoblastic leukaemia. *Br J Haematol* 2010; **150**: 665–673.
28 Aldana-Masangkay GI, Rodriguez-Gonzalez A, Lin T, Ikeda AK, Hsieh Y-T, Kim Y-M *et al.* Tubacin suppresses proliferation and induces apoptosis of acute lymphoblastic leukemia cells. *Leuk Lymphoma* 2011; **52**: 1544–1555.
29 Huang C, Hu X, Wang L, Lü S, Cheng H, Song X *et al.* Bortezomib suppresses the growth of leukemia cells with *Notch1* overexpression *in vivo* and *in vitro*. *Cancer Chemother Pharmacol* 2012; **70**: 801–809.
30 Chou TC. Drug combination studies and their synergy quantification using the Chou-Talalay method. *Cancer Res* 2010; **70**: 440–446.
31 Wada T, Kikuchi J, Furukawa Y. Histone deacetylase 1 enhances microRNA processing *via* deacetylation of DGCR8. *EMBO Rep* 2012; **13**: 142–149.
32 Renard P, Ernest I, Houbion A, Art M, Le Calvez H, Raes M *et al.* Development of a sensitive multi-well colorimetric assay for active NFκB. *Nucleic Acid Res* 2001; **29**: e21.
33 Kikuchi J, Shibayama N, Yamada S, Wada T, Nobuyoshi M, Izumi T *et al.* Homopiperazine derivatives as a novel class of proteasome inhibitors with a unique mode of proteasome binding. *PLoS One* 2013; **8**: e61649.
34 Kikuchi J, Yamada S, Koyama D, Wada T, Nobuyoshi M, Izumi T *et al.* The novel orally active proteasome inhibitor K-7174 exerts anti-myeloma activity *in vitro* and *in vivo* by down-regulating the expression of class I histone deacetylases. *J Biol Chem* 2013; **288**: 25593–25602.
35 Nakahara F, Sakata-Yanagimoto M, Komeno Y, Kato N, Uchida T, Haraguchi K *et al.* Hes1 immortalizes committed progenitors and plays a role in blast crisis transition in chronic myelogenous leukemia. *Blood* 2010; **115**: 2872–2881.
36 van Hamburg JP, de Bruijn MJW, Dingjan GM, Beverloo HB, Diepstraten H, Ling K-W *et al.* Cooperation of Gata3 c-Myc and Notch in malignant transformation of double positive thymocytes. *Mol. Immunol* 2008; **45**: 3085–3095.
37 Giambra V, Jenkins CR, Wang H, Lam SH, Shevchuk OO, Nemirovsky O *et al.* NOTCH1 promotes T cell leukemia-initiating activity by RUNX-mediated regulation of PKC-θ and reactive oxygen species. *Nat Med* 2012; **18**: 1693–1698.
38 Chang P-Y, Draheim K, Kelliher MA, Miyamoto S. NFKB1 is a direct target of the TAL1 oncoprotein in human T leukemia cells. *Cancer Res* 2006; **66**: 6009–6013.
39 Vilimas T, Mascarenhas J, Palomero T, Mandal M, Buonamici S, Meng F *et al.* Targeting the NF-κB signaling pathway in Notch1-induced T-cell leukemia. *Nat Med* 2007; **13**: 70–77.
40 Lambertini C, Pantano S, Dotto GP. Differential control of Notch1 gene transcription by Klf4 and Sp3 transcription factors in normal versus cancer-derived keratinocytes. *PLoS One* 2010; **5**: e10369.
41 Blume SW, Snyder RC, Ray R, Thomas S, Koller CA, Miller DM. Mithramycin inhibits SP1 binding and selectively inhibits transcriptional activity of the dihydrofolate reductase gene *in vitro* and *in vivo*. *J Clin Invest* 1991; **88**: 1613–1621.
42 Deacon K, Onion D, Kumari R, Watson SA, Knox AJ. Elevated SP-1 transcription factor expression and activity drives basal and hypoxia-induced vascular endothelial growth factor (VEGF) expression in non-small cell lung cancer. *J Biol Chem* 2012; **287**: 39967–39981.
43 Gu L, Findley HW, Zhou M. MDM2 induces NF-κB/p65 expression transcriptionally through Sp1-binding sites: a novel, p53-independent role of MDM2 in doxorubicin resistance in acute lymphoblastic leukemia. *Blood* 2002; **99**: 3367–3375.
44 Cohen LY, Bourbonnière M, Sabbagh L, Bouchard A, Chew T, Jeannequin P *et al.* Notch1 antiapoptotic activity is abrogated by caspase cleavage in dying T lymphocytes. *Cell Death Differ* 2005; **12**: 243–254.
45 Zheng L, Saunders CA, Sorensen EB, Waxmonsky NC, Conner SD. Notch signaling from the endosome requires a conserved dileucine motif. *Mol Biol Cell* 2013; **24**: 297–307.
46 Wang YT, Yang WB, Chang WC, Hung JJ. Interplay of posttranslational modifications in Sp1 mediates Sp1 stability during cell cycle progression. *J Mol Biol* 2011; **414**: 1–14.
47 Shin HM, Minter LM, Cho OH, Gottipati S, Fauq AH, Golde TE *et al.* Notch1 augments NF-κB activity by facilitating its nuclear retention. *EMBO J* 2006; **25**: 129–138.
48 Hideshima T, Chauhan D, Kiziltepe T, Ikeda H, Okawa Y, Podar K *et al.* Biologic sequelae of IκB kinase (IKK) inhibition in multiple myeloma: therapeutic implications. *Blood* 2009; **113**: 5228–5236.
49 Lovén J, Hoke HA, Lin CY, Lau A, Orlando DA, Vakoc CR *et al.* Selective inhibition of tumor oncogenes by disruption of super-enhancers. *Cell* 2013; **153**: 320–334.
50 Fulciniti M, Amin S, Nanjappa P, Rodig S, Prabhala R, Li C *et al.* Significant biological role of Sp1 transactivation in multiple myeloma. *Clin Cancer Res* 2011; **17**: 6500–6509.



Supplementary Information accompanies this paper on the Leukemia website (http://www.nature.com/leu)

Oncogene (2014), 1–9

www.nature.com/onc

ORIGINAL ARTICLE

# Arf tumor suppressor disrupts the oncogenic positive feedback loop including c-Myc and DDX5

K Tago[1], M Funakoshi-Tago[2], H Itoh[3], Y Furukawa[4], J Kikuchi[4], T Kato[5], K Suzuki[5] and K Yanagisawa[1]

Tumor suppressor protein $p19^{ARF}$ (Arf; $p14^{ARF}$ in humans) functions in both p53-dependent and -independent modes to counteract hyper-proliferative signals caused by proto-oncogene activation, but its p53-independent activities remain poorly understood. Using the tandem affinity purification-tag technique, we purified Arf-containing protein complexes and identified p68 DEAD-box protein (DDX5) as a novel interacting protein of Arf. In this study, we found that DDX5 interacts with c-Myc, and harbors essential roles for c-Myc-mediated transcription and its transforming activity. Furthermore, when c-Myc was forcibly expressed, the expression level of DDX5 protein was drastically increased through the acceleration of protein synthesis of DDX5, suggesting the presence of an oncogenic positive feedback loop including c-Myc and DDX5. Strikingly, Arf blocked the physical interaction between DDX5 and c-Myc, and drove away DDX5 from the promoter of c-Myc target genes. These observations most likely indicate the mechanism by which Arf causes p53-independent tumor-suppressive activity.

*Oncogene* advance online publication, 27 January 2014; doi:10.1038/onc.2013.561

**Keywords:** Arf; c-Myc; DDX5

## INTRODUCTION

The *INK4a–ARF* locus (*CDKN2A* in humans) encodes two intimately linked but distinct tumor suppressor proteins, $p16^{Ink4a}$ and $p19^{ARF}$ (Arf; $p14^{ARF}$ in humans), which indirectly contribute to the activation of the retinoblastoma protein and the p53 transcription factor, respectively.[1–3] Arf protein is a potent tumor suppressor that blocks cell cycle progression by directly binding to, and interfering with, the p53-negative regulator Mdm2, thereby stabilizing and activating p53.[4–6] Additionally, p53 is also regulated by other ubiquitin E3-ligases, such as COP1 and ARF-BP1/Mule (HectH9), and the activity of ARF-BP1 is antagonized by Arf.[7,8]

It is generally accepted that the tumor-suppressive activity of Arf is mainly mediated through p53; however, Arf is also known to have p53-independent functions. The research investigating the carcinogen-induced papillomas in Arf- and p53-deficient mice has suggested that Arf inhibits the proliferative rate of tumors in a p53-independent manner, and enforced expression of Arf can arrest the proliferation of p53-deficient cells, although less efficiently than in cells that retain wild-type p53.[9,10] Primary murine embryo fibroblasts (MEFs) and B lymphocytes lacking both *Arf* and *p53* grow faster in culture than cells lacking only one of the two genes, and mice lacking *Arf, Mdm2* and *p53* are much more prone to developing cancer than mice lacking *Mdm2* and *p53*.[3,11,12] Although the detailed mechanisms still remain to be elucidated, Arf inhibits ribosomal RNA processing in a p53-independent manner, and this most likely involves a nucleolar protein, nucleophosmin (NPM).[13–15] Forcibly expressed Arf also suppresses the transcriptional activities of E2Fs, c-Myc and NF-κB; however, these p53-independent activities of Arf are relatively poorly understood.[16–20] Notably, the enforced expression of Arf also promotes the SUMOylation of several proteins to which Arf binds without affecting the p53 activation.[21,22] Arf-induced SUMOylation is mediated by its ability to antagonize SENP3, a SUMO-specific protease.[23] However, the role of Arf-induced SUMOylation has yet to be clarified.

p68 RNA helicase (also called DEAD-box protein 5; DDX5) is a member of the DEAD-box family of RNA helicases.[24] DDX5 is one of the first DEAD-box family proteins to be shown to exhibit RNA helicase activity *in vitro*, and it plays a very important role in cell proliferation and early organ development and maturation.[25–27] The protein displays cell cycle-related alteration of localization in the nucleus. Related to the role of DDX5 in cell proliferation, the expression of the protein was shown to correlate with tumor progression and transformation.[28–30] In response to platelet-derived growth factor (PDGF) stimulation, DDX5 is phosphorylated by tyrosine kinase c-Abl, and phosphorylated DDX5 promotes epithelial—mesenchymal transition via promotion of the nuclear translocation of β-catenin.[31] Recently, DDX5 was identified as one of the proteins whose expression is increased in Arf-deficient cells, and it was also shown that DDX5 participates in ribosome biogenesis in collaboration with NPM.[32]

In the current study, we identified DDX5 as a novel component of Arf complexes. Furthermore, we discovered the presence of an oncogenic positive feedback loop between c-Myc and DDX5, and Arf disrupts this interaction to block c-Myc-induced cellular transformation. In this study, we found that DDX5 is one of the critical mediators of the p53-independent tumor-suppressive pathways induced by Arf.

[1]Division of Structural Biochemistry, Department of Biochemistry, School of Medicine, Jichi Medical University, Shimotsuke-shi, Japan; [2]Faculty of Pharmacy, Department of Biochemistry, Keio University, Minato-ku, Japan; [3]Laboratory of Signal Transduction, Department of Cell Biology, Graduate School of Biological Sciences, Nara Institute of Science and Technology, Ikoma, Japan; [4]Division of Stem Cell Regulation, Center for Molecular Medicine, Jichi Medical University, Shimotsuke-shi, Japan and [5]Department of Surgery, Saitama Medical Center, Jichi Medical University, Omiya-ku, Japan. Correspondence: Dr K Tago, Division of Structural Biochemistry, Department of Biochemistry, School of Medicine, Jichi Medical University, 3311-1 Yakushiji, Shimotsuke-shi, 329-0498 Tochigi, Japan.
E-mail: ktago@jichi.ac.jp
Received 7 June 2013; revised 1 November 2013; accepted 25 November 2013

## RESULTS

### Identification of DDX5 as a novel Arf-interacting protein

To identify novel targets for Arf, we constructed a retroviral vector harboring $p19^{ARF}$ tagged with C-terminal FLAG and His epitopes (Arf-FLAG/His), and infected this into NIH-3T3 cells. The nuclear extracts from the infected cells were sequentially subjected to affinity chromatography on M2 (FLAG antibody) agarose beads and Ni-NTA agarose (Figure 1a). A number of proteins were copurified with Arf-FLAG/His (Figure 1b), and MudPIT mass spectrometry analyzing these interacting proteins revealed that Arf bound to many known and unknown proteins (Supplementary Table S1). Among them, we identified B23/NPM, a known Arf-binding protein, as a specific component of the Arf complexes (Figure 1c).[14,15] We also identified DDX5 as a novel binding partner of Arf, and DDX5 was also detected in Arf complexes by immunoblot analysis (Figure 1c). Thus far, in our mass spectrometry analysis, we could not detect the interacting proteins reported previously, such as HECTH9 and c-Myc.[7,18]

### Arf binds to catalytic domain of DDX5

Several functional domains have been mapped within DDX5 (Figure 2a). The central domain, called the DEAD box, is an ATPase catalytic domain. RGS-RGG domain and IQ motif lie at the C terminus. We generated a series of deletion mutants of FLAG-tagged DDX5 and transiently expressed them with/without Arf in 293T cells. Then, we determined which domain of DDX5 is required for the interaction with Arf by performing immunoprecipitation. Arf bound to the N134, C430 and C554 mutants but not to ΔCat mutant lacking an ATPase catalytic domain (Figure 2b). We also analyzed the interaction between DDX5 and NPM (Figure 2b, bottom photograph). Interestingly, DDX5 also bound to NPM; however, Arf diminished this interaction, as previously reported.[32] Furthermore, the mode of interaction between DDX5 and NPM is most likely different from the case of DDX5 and Arf. Whereas Arf binds to the ATPase catalytic domain of DDX5, the interaction of DDX5 with NPM seems to be mediated by multiple domains of DDX5, except its C-terminal IQ motif. Furthermore, we prepared the recombinant proteins of DDX5 and GST-Arf, and performed *in vitro* pulldown assay. As shown in Figure 2c, Arf directly bound to DDX5.

### Arf inhibits DDX5-mediated c-Myc activation

Arf antagonizes the function of a proto-oncogene product, c-Myc, in a p53-independent manner.[18,19] Therefore, we next investigated the functional involvement of DDX5 in the transcriptional activity of c-Myc. As shown in Figure 3a, we infected TKO cells lacking three genes of Arf, p53 and Mdm2 with retrovirus harboring Myc-ER. Myc-ER is a fusion protein of c-Myc with a ligand-binding domain of estrogen receptor, and its activation is induced by addition of an estrogen analog, 4-hydroxytamoxifen (4-HT).[33,34] When Myc-ER was expressed, 4-HT induced the expression of target genes of c-Myc such as Odc, cyclin D2 and spermidine synthase, and these were effectively impeded by Arf (Figure 3a shows the expression of Myc-ER, Arf, DDX5 and β-actin; Figures 3b–d show the results of quantitative PCR). We next tested the effect of DDX5 knockdown on the transcriptional activity of Myc-ER. Strikingly, the knockdown of DDX5 also suppressed the expression of Odc, cyclin D2 and spermidine synthase induced by Myc-ER (Figures 3b–d). This strongly suggests that DDX5 is important for the transcriptional activity of c-Myc. Next, we induced the expression of c-Myc and DDX5 in HEK293T cells, and performed an immunoprecipitation assay to test whether DDX5 can form a complex with c-Myc. As shown in Figure 4a, DDX5 bound to c-Myc. Furthermore, to decide which domain of DDX5 is required for the interaction with c-Myc, we performed the immunoprecipitation assay using the same series of deletion mutants of DDX5 as shown in Figure 2a. As c-Myc failed to bind to C430 and C554, it is suggested that c-Myc interacts with DDX5 through C-terminal domain including IQ motif. To gain further insight for the mechanism how ARF inhibits the transcriptional activity of c-Myc, we tested the effect of ARF on the interaction between DDX5 and c-Myc. Interestingly, this interaction was markedly reduced by Arf (Figure 4b). Furthermore, it should be mentioned that we failed to detect the interaction of DDX5 with a transcriptional activator of c-Myc, TIP49 (Supplementary Figure S1). These results suggest that Arf exhibits p53-independent tumor-suppressive activity by sequestering DDX5 from protein complexes of c-Myc. To confirm this possibility, we performed chromatin immunoprecipitation assay. We infected TKO cells with retroviruses harboring c-Myc with/without Arf. As shown in Figures 4c and d, the expression of c-Myc resulted in the recruitment of DDX5 onto the promoter region of Odc. The forced expression of Arf effectively inhibited this recruitment of

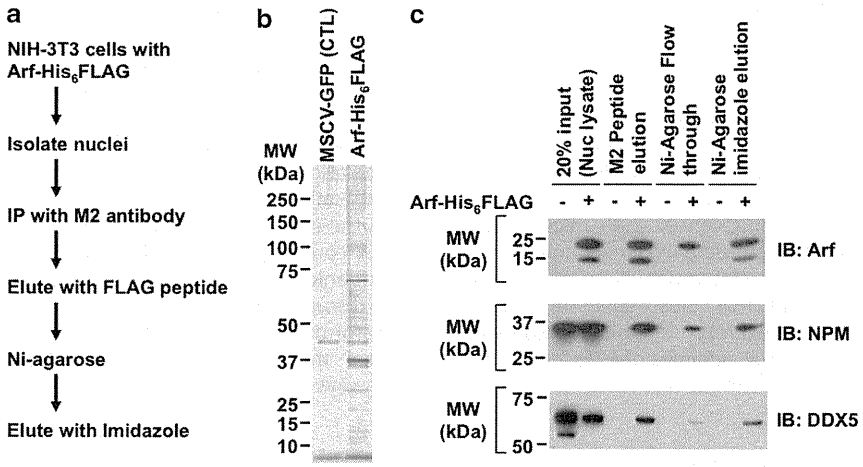


**Figure 1.** Identification of DDX5 as an interacting protein of Arf. (**a**) The method of purification of the protein complexes containing Arf by performing tandem affinity purification-tag technique is described. (**b**) The protein complexes containing Arf were dissolved by SDS–polyacrylamide gelelectrophoresis (5–20% gradient) and subjected to silver staining. Control (CTL) samples were purified from the cells infected with control retrovirus (MSCV–IRES–GFP). (**c**) Immunoblot analysis of the protein complexes containing Arf with the antibodies against Arf, NPM and DDX5. Input samples (nuclear lysate), first purified samples (M2 agarose), flow-through fractions of Ni-agarose, and eluted fractions of Ni-NTA (second purified samples) were analyzed.

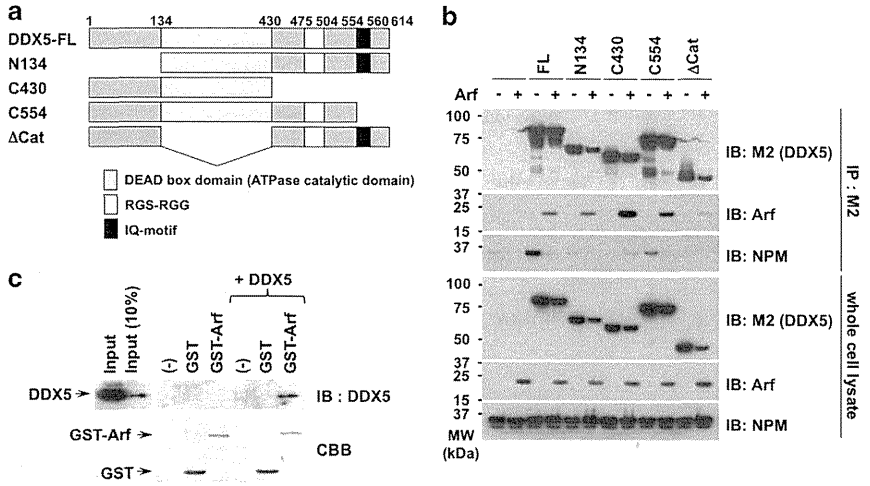


**Figure 2.** DDX5 directly interacts with Arf, mediated by its catalytic domain. (**a**) Schematic representations of wild-type and deletion mutants of DDX5 are shown by describing each functional motif and numbers corresponding to the amino-acid residues. (**b**) In HEK293T cells, Arf and full-length and deletion mutants of DDX5 were expressed, and then immunoprecipitation of DDX5 was performed with M2 antibody. The interaction of Arf and NPM with full-length and deletion mutants of DDX5 was analyzed by immunoblotting with anti-Arf, anti-NPM or M2 antibodies. (**c**) GST-Arf (or control GST) and His-DDX5 were mixed and incubated for 30 min at 25 °C. Then, protein complexes were captured with glutathione sepharose, and analyzed by immunoblotting.

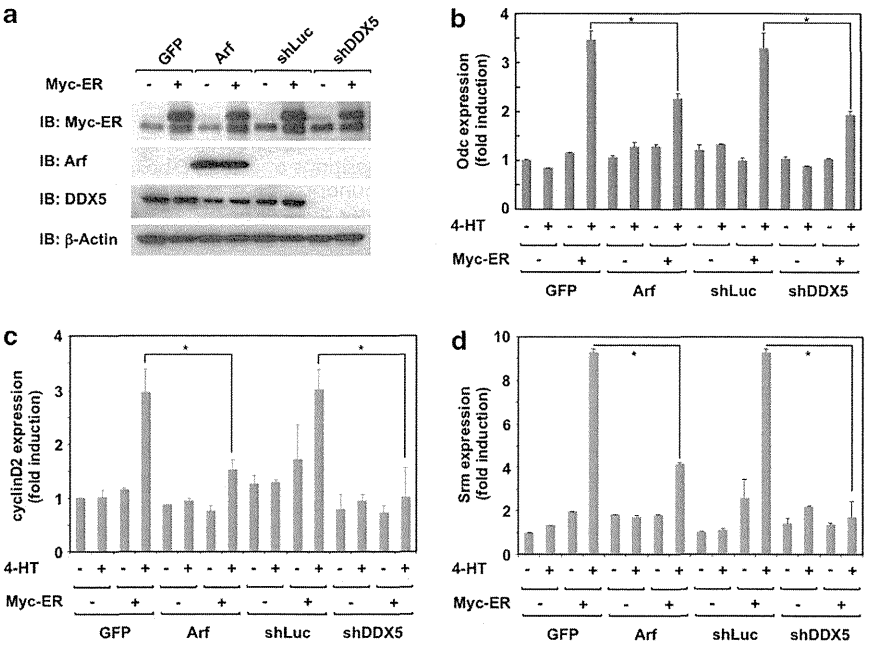


**Figure 3.** DDX5 is required for the transcriptional activity of c-Myc. (**a**) TKO cells were infected with the indicated combination of retroviruses harboring sh-luciferase (shLuc), shDDX5, Arf and/or c-Myc fused protein Myc-ER. Cell lysates were analyzed by immunoblotting with the indicated antibodies. (**b**–**d**) TKO cells infected with the indicated combinations of retroviruses were treated with 1 μM 4-HT, and 12 h later, total RNA was prepared and used for quantitative PCR for Odc (**b**), cyclin D2 (**c**) and spermidine synthase (**d**). In the graph, error bars mean s.d. ($n=3$, $^*P<0.01$).

DDX5 on the Odc promoter. These results strongly suggest that Arf interrupts the complex formation of DDX5 and c-Myc, and this could be a crucial mechanism by which Arf inhibits c-Myc in a p53-independent manner.

## Arf suppresses the oncogenic positive feedback loop including DDX5 and c-Myc

Next, we investigated whether DDX5 contributes to c-Myc-induced transformation. Interestingly, c-Myc enhanced the expression of DDX5 protein, when c-Myc was ectopically expressed in TKO cells (Figure 5a). However, Arf inhibited the c-Myc-induced enhancement of DDX5 expression. Using the series of infected MEFs, we then analyzed the effect of Arf and knockdown of DDX5 on the c-Myc-induced acceleration of cell proliferation. As shown in Figure 5b, Arf and the knockdown of DDX5 effectively suppressed the cell proliferation rate enhanced by c-Myc, although the suppressive efficiency was not drastic like the inhibitory effects on the transcriptional activity of Myc-ER as shown in Figure 4. Interestingly, Arf inhibited the c-Myc-induced

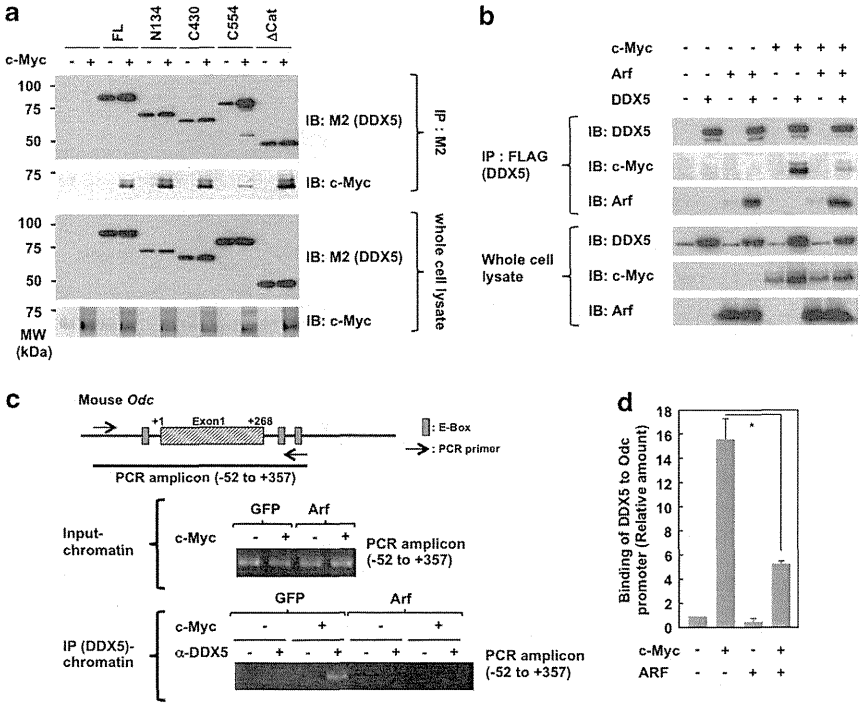


**Figure 4.** Arf blocks the functional interaction between c-Myc and DDX5. (**a**) Full-length or deletion mutants of DDX5 and c-Myc were expressed in HEK293T cells and then, immunoprecipitation of DDX5 was performed with M2 antibody. The interaction of c-Myc with full-length and deletion mutants of DDX5 was analyzed by immunoblotting with anti-c-Myc and M2 antibodies, respectively. (**b**) HEK293T cells were transfected with the indicated combination of plasmids encoding Arf, FLAG-DDX5 and c-Myc. Their cell lysates were used for immunoprecipitation with anti-FLAG (M2) antibody. Immunoprecipitates and whole cell lysates were analyzed by immunoblotting with anti-Arf, anti-DDX5 and anti-c-Myc antibodies. (**c**) TKO cells infected with the indicated combination of retroviruses harboring Arf and c-Myc were used for the chromatin immunoprecipitation with anti-DDX5 antibody. The positions of exon1, E-box sequences and primers were indicated. The chromatin fragments included in whole cell lysates (input) and the immunoprecipitated chromatin were used as the template for PCR using the primers for the E-box sequence of a c-Myc target gene, *Odc*. The intensities of bands are shown in graph as relative amounts in **d**. Error bars mean s.d. ($n = 3$, $^*P < 0.01$).

transformation of TKO cells (Figures 5c and d). The reduction of DDX5 expression by short hairpin RNA also impeded c-Myc-induced transformation of TKO cells. Combining these observations with the results shown in Figure 4, Arf is supposed to inhibit c-Myc-induced transcription and transformation mediated by blocking the physical and functional interaction between DDX5 and c-Myc in a p53-independent manner. Next, to determine whether c-Myc-transformed fibroblasts can exhibit tumor formation with Arf or without DDX5 *in vivo*, TKO cells transduced with/without c-Myc and Arf, shLuc (sh-luciferase; control) or shDDX5 were subcutaneously. inoculated into the flanks of nude mice. As shown in Figures 6a and b, c-Myc causes tumor formation in nude mice, and this was effectively reduced by the induced expression of Arf or knockdown of DDX5. When the tumors were isolated and their volumes were measured, the expression of Arf or knockdown of DDX5 apparently reduced the tumor growth induced by c-Myc (Figures 6c and d). These findings demonstrated that DDX5 contributes to c-Myc-induced tumorigenesis not only *in vitro* but also *in vivo*, and Arf inhibits the tumor formation by c-Myc.

## c-Myc and DDX5 are correspondingly expressed in leukemia and colon cancers

We analyzed the protein expression levels of c-Myc and DDX5 in various solid tumor cell lines by immunoblotting. In some cases (MCF-7, HeLa, Neuro-2A and S49), DDX5 was highly expressed, and this was well correlated with the expression level of c-Myc (Supplementary Figure S2), supporting our hypothesis of an oncogenic feedback loop including c-Myc and DDX5. Furthermore, we analyzed the expression levels of DDX5 and c-Myc proteins in 13 leukemia cell lines and samples from colon cancer patients ($n = 8$). In the leukemia cell lines, the expression level of DDX5 was well correlated with the c-Myc expression (Figure 7a). We also analyzed the expression level of κB-Ras2, as a control, and κB-Ras2 expression was not correlated with c-Myc or DDX5. We measured the expression level of these proteins, and showed the correlation of their expression levels in a graph. As a result, c-Myc and DDX5 showed an intermediate positive correlation, whereas κB-Ras2 failed to show an expressional correlation with c-Myc (Figure 7b). Furthermore, in the cases of colon cancer patients, high expression of c-Myc and DDX5 was only observed in tumor, but not in normal tissues (Figure 7c). These findings strongly support our model of an oncogenic positive feedback loop including c-Myc and DDX5.

## c-Myc accelerates the protein synthesis of DDX5

Combining the result shown in Figure 5a and the observation that DDX5 is required for the action of c-Myc, suggesting the presence of an oncogenic positive feedback loop including c-Myc and DDX5, we attempted to clarify the mechanism by which c-Myc causes high expression of DDX5. First, we tested whether DDX5 is a target gene of c-Myc by performing reverse transcription–PCR using Myc-ER system. However, we could not observe the induction of the DDX5 mRNA expression by Myc-ER (Figure 8a). We next tested whether the transcriptional activity of c-Myc is required for c-Myc-induced enhancement of DDX5 expression. The wild-type c-Myc, its constitutively active mutant (T58A) and its inactive mutant, In373, were overexpressed in TKO cells, and the

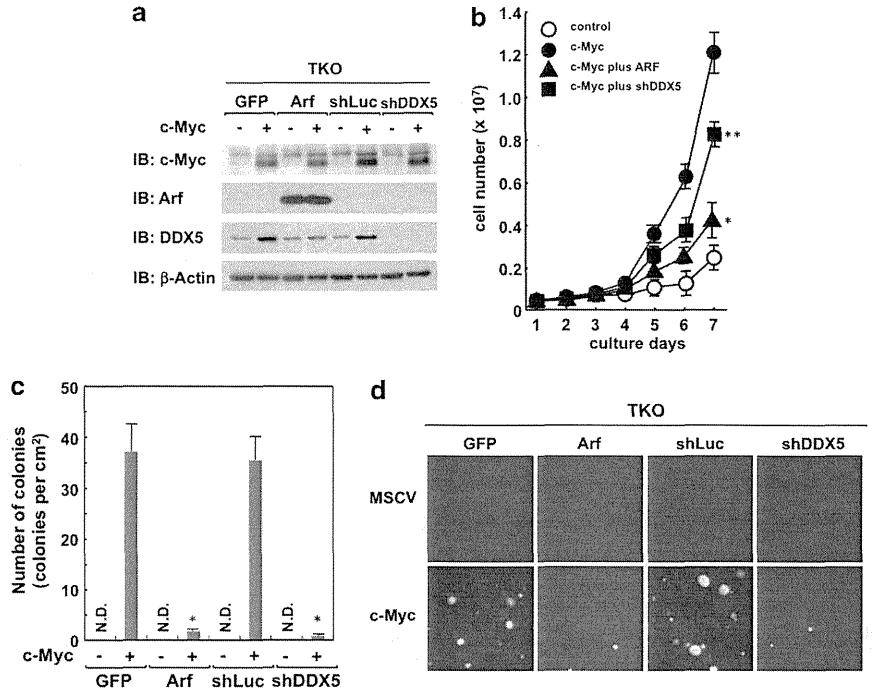


**Figure 5.** Arf expression and DDX5 knockdown inhibits c-Myc-induced transformation. TKO cells were infected with the indicated combinations of retroviruses harboring sh-luciferase, shDDX5, Arf and/or c-Myc. (**a**) Cell lysates were analyzed by immunoblotting with the indicated antibodies. (**b**) TKO cells infected with the indicated combinations of retroviruses were seeded on 60-mm-diameter dishes ($1 \times 10^4$ cells/dish), and cell proliferations were evaluated during 7 days. (**c**) Infected TKO cells were used for the soft agar colony formation assay to evaluate the involvement of Arf and DDX5 in c-Myc-induced transformation. (**d**) The number of colonies of transformed TKO cells counted in **c** is shown in the graph. Error bars mean s.d. ($n = 3$, $^*P < 0.01$, $^{**}P < 0.02$).

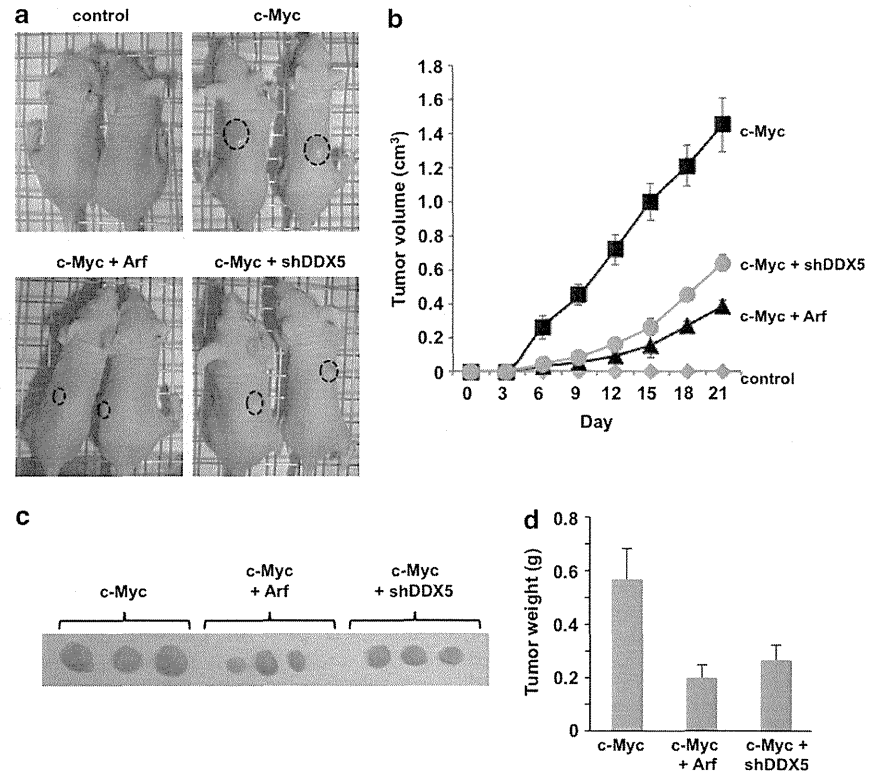


**Figure 6.** Effects of Arf and DDX5 on the c-Myc-induced tumor formation *in vivo*. (**a**) TKO cells infected with the indicated combinations of retroviruses harboring sh-luciferase, shDDX5, Arf and/or c-Myc (a total of $2 \times 10^6$ cells) were utilized for subcutaneous injection into nude mice. Fifteen days later, tumor formation in mice was shown. (**b**) Tumor burden was monitored over a 21-day period, and the results are shown graphically. (**c**) At the end of the experiments, mice were killed and tumors were isolated, as shown in the photograph. Each tumor's weight was measured and is shown in the graph (**d**). Error bars mean s.d. ($n = 3$).